Inorganica Chimica Acta 474 (2018) 51–65

Contents lists available at ScienceDirect

Inorganica Chimica Acta

journal homepage: www.elsevier.com/locate/ica

Research paper

spiro-Cyclotriphosphazenes containing 4-hydroxyphenylethyl pendant arm: Syntheses, structural characterization and DNA interaction study

Serhan Pektaş [a], Selen Bilge Koçak [a,*], Nisan Sevin Başterzi [a], Zeynel Kılıç [a], Celal Tuğrul Zeyrek [b], Burak Coban [c], Ufuk Yildiz [c], Ömer Çelik [d]

[a] Department of Chemistry, Ankara University, 06100 Tandoğan, Ankara, Turkey
[b] Department of Training and Application, Ankara Nuclear Research and Training Center, Turkish Atomic Energy Authority, 06100 Beşevler, Ankara, Turkey
[c] Department of Chemistry, Bülent Ecevit University, 67100 Incivez, Zonguldak, Turkey
[d] Department of Physics, Dicle University, 21280 Sur, Diyarbakır, Turkey

ARTICLE INFO

Article history:
Received 24 July 2017
Received in revised form 25 December 2017
Accepted 18 January 2018

Keywords:
spiro-Cyclotriphosphazenes
Tyramine
Spectroscopy
DNA interaction
Molecular docking

ABSTRACT

The reaction of hexachlorocyclotriphosphazene, $N_3P_3Cl_6$, with tyramine podand (**2**) afforded partly substituted *spiro*-cyclotriphosphazene (**3**). Amine-substituted *spiro*-cyclotriphosphazenes **4a–g** were prepared by substitution of the Cl–atoms in **3** with pyrrolidine, piperidine, morpholine, 1,4-dioxa-8-azaspiro[4,5]decane, 1-(2-aminoethyl)pyrrolidine, 1-(2-aminoethyl) piperidine, and 4-(2-aminoethyl)-morpholine, respectively. All of the cyclotriphosphazene derivatives were characterized by elemental analysis, FTIR, MS, 1D ^1H, ^{13}C and ^{31}P NMR and 2D HSQC techniques, and the crystal structures of **3** and **4b** were verified by X-ray diffraction analysis. The relationships δP_{OPN} shifts with exocyclic OPN (α') and endocyclic NPN (α) bond angles, and electron density transfer parameters Δ(P-N) for *spiro*-cyclotriphosphazenes were presented. The DNA cleavage activity of cyclotriphosphazene derivatives (**3**, and **4a–g**) was studied on double-stranded pBR322 DNA using gel electrophoresis experiments. It was found that **4e** and **4f** caused the highest level of DNA damage. The interactions of **3** and **4e** with calf thymus DNA were also investigated using absorption spectrometry. The molecular docking was performed to identify the interaction of the compounds (**3** and **4b**) with the DNA (PDB ID:3V9D for A-DNA and PDB ID:1BNA for B-DNA).

1. Introduction

Cyclophosphazenes are one of the most studied inorganic ring compounds, consisting of the repeating unit $[NPR_2]_n$ (n = 3, 4, 5,...), and two side-groups (R) of organic, inorganic, and organometallic type [1]. Among these compounds, hexachlorocyclotriphosphazene (cyclic trimer, $N_3P_3Cl_6$) has received particular interest in phosphazene-based chemistry because it is a versatile starting compound for the syntheses of cyclotriphosphazene derivatives [2], dendrimers [3], and polyphosphazenes [4]. Generally, cyclotriphosphazenes have been obtained substituting the Cl-atoms in $N_3P_3Cl_6$ with —NH or —OH functionalized nucleophilic reagents, including primary [5] and secondary [6] amines, phenoxides [7], and N/N [8] and N/O [9,10] bifunctional reagents. The presence of —P=N— structural units in the backbone and the variety of side groups (same or different) attached to the P-atoms makes cyclotriphosphazenes potentially useful in a wide variety of applications such as ionic liquids [11], liquid crystals [12], flame-retardants [13], light-emitting diodes [14], and electrolytes for lithium-ion batteries [15].

Tyramine [4-(2-aminoethyl)phenol, 4-hydroxyphenethylamine, mydrial or uteramine] is a biogenic and trace amine, which is widely used as a pharmacological tool to evaluate the role of the sympathetic nervous system in human physiology and pathology [16]. Tyramine is responsible for some food-induced migraines and the hypertensive crisis that may occur in sensitive individuals with monoamine oxidase inhibitor drugs [17]. Tyramine is generated by decarboxylation of the amino acid tyrosine through tyrosine decarboxylase enzyme derived from the bacteria present in the food. The ingestion of food containing high levels of tyramine causes tyramine poisoning [18]. The physiological effects of tyramine include peripheral vasoconstriction, increased cardiac output, increased respiration, elevated blood glucose, and release of norepinephrine [19]. Tyramine is also a neuroactive chemical in insects (and probably mammals also), where it has been found to affect a wide spectrum of behaviors, including locomotion, foraging, aggression, and learning [20]. The tyramine-derived Schiff base

* Corresponding author.
E-mail address: sbilge@science.ankara.edu.tr (S. Bilge Koçak).

https://doi.org/10.1016/j.ica.2018.01.016
0020-1693/

ligands and their metal complexes have been identified to as promising DNA binding and antibacterial agents [21].

To the best of our knowledge, some reports have appeared on phosphazene derivatives containing the tyramine moiety [22]. The present study focused primarily on the synthesis and structural determination of *spiro*-cyclotriphosphazenes with a nitrogen-attached 4-hydroxyphenylethyl pendant arm, which was formed by incorporation of a tyramine unit into the cyclotriphosphazene skeleton to give partly substituted phosphazene (**3**). A series of fully substituted phosphazenes (**4a**–**g**) was obtained by the substitution of the Cl–atoms in **3** with heterocyclic amines [pyrrolidine (Pyr), piperidine (Pip), morpholine (Morp), 1,4-dioxa-8-azaspiro[4,5]decane (DASD), 1-(2-aminoethyl)pyrrolidine (AEPyr), 1-(2-aminoethyl) piperidine (AEPip), and 4-(2-aminoethyl)morpholine (AEMorp)] (Scheme 1). Recent investigations have shown that cyclotriphosphazene derivatives exhibit potential DNA-interacting properties [23] and antimicrobial activities [24]. It is well known that mono- and poly amino-substituted cyclotriphosphazenes have potential value in cancer therapies [25].

Prompted by the above observations, it seemed worthwhile to investigate if the presence of the tyramine moiety and/or the heterocyclic amine groups on the cyclotriphosphazene skeleton gives rise to a new class of biologically active molecules such as DNA binders. The principal reason for selecting tyramine podand (**2**) as the ligand, when attached to $N_3P_3Cl_6$, was the formation of 4-hydroxyphenylethyl pendant arm in a *spiro*-structure, and that the pendant arm OH group was expected to be able to bind DNA via hydrogen bonds and with the help of the planar phenyl ring as an intercalator. The addition of heterocyclic amines, which can be protonated at physiological pH, to the structure may also give better affinity through binding to the negatively charged DNA. Characterization of the cyclotriphosphazenes (**3** and **4a**–**g**) was carried out by elemental analysis, mass spectrometry (MS), Fourier transform infrared (FTIR), one-dimensional (1D) ^{1}H, ^{13}C, and ^{31}P NMR spectroscopy, and two-dimensional (2D) heteronuclear single-quantum correlation (HSQC) techniques. The crystal structures of partly- (**3**) and fully Pip- (**4b**) substituted *spiro*-cyclotriphosphazenes were also determined using X-ray crystallography. The relationships δP_{OPN} shifts and exocyclic OPN (α') and endocyclic NPN (α) bond angles, and the correlations of electron density transfer parameters Δ(P-N) with δP_{OPN} shifts were investigated using ^{31}P NMR and X-ray data. The DNA binding propensity of the synthesized compounds were studied. Molecular docking calculations using AutoDock Vina software were carried out to predict the mode of interaction of the compounds with DNA.

2. Experimental

2.1. Materials used for synthesis

Commercial-grade reagents were used without further purification, and solvents were dried and distilled by standard methods. The solvents, salicylaldehyde, sodium borohydride, borax and potassium carbonate were purchased from Merck, while (Pyr, Pip, Morp, DASD), and (AEPyr, AEPip, and AEMorp) were purchased from Merck and Sigma Aldrich, respectively. Hexachlorocyclotriphosphazene, $N_3P_3Cl_6$ (Alfa Easar) was purified by fractional crystallization from *n*-hexane, and all reactions were monitored using thin-layer chromatography (TLC) on Merck DC Alufolien Kieselgel 60 B_{254} sheets. Column chromatography was performed on Merck Kieselgel 60 (230–400 mesh ATSM) silica gel, and all reactions were conducted under an argon atmosphere.

2.2. Physical methods

Melting points were measured with a Gallenkamp apparatus using a capillary tube. Microanalyses (C, H, N) were performed using a Leco CHNS-932 elemental analyzer at the Central Instrumental Analysis Laboratory in the Faculty of Pharmacy at Ankara University. ^{1}H (400 MHz) and ^{13}C (100 MHz) NMR, and HSQC spectra were recorded employing a Varian Mercury 400 MHz FT spectrometer, while ^{31}P NMR spectra were obtained by using a Bruker DPX FT-NMR 500 MHz spectrometer; $SiMe_4$ was used as an internal standard for ^{1}H and ^{13}C NMR and external 85% H_3PO_4 for ^{31}P NMR. FTIR spectra of the compounds were recorded on a Shimatzu infinity model FTIR spectrometer connected to 3 reflective ATR devices. ESI-MS mass spectra were obtained on an Agilent 1100 MSD spectrometer.

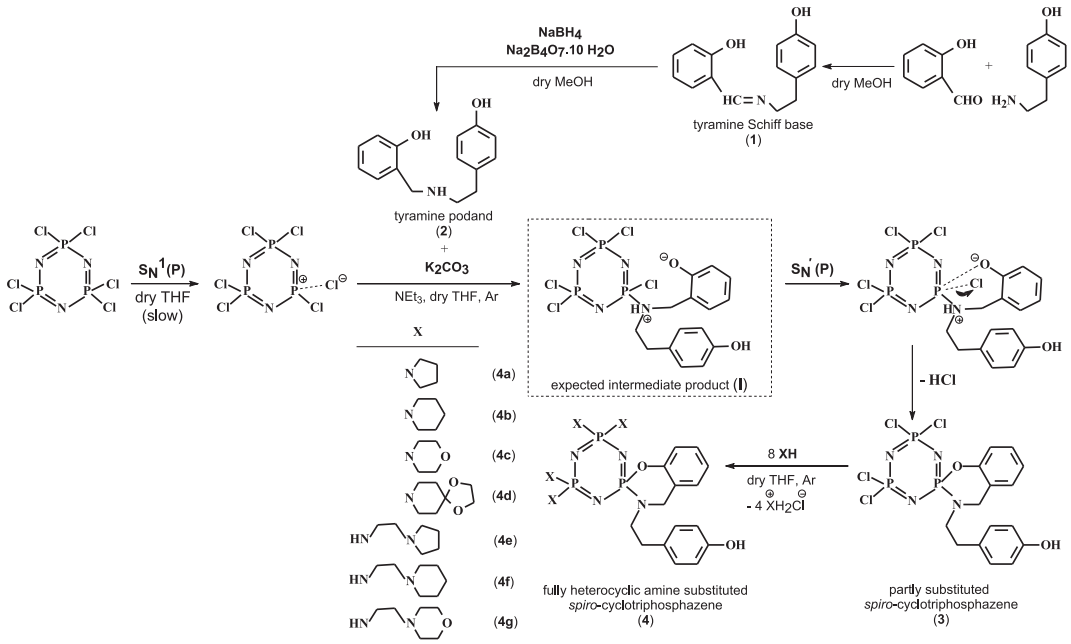

Scheme 1. Reaction pathways of $N_3P_3Cl_6$ with tyramine podand (**2**) and fully substituted (**4a**–**g**) *spiro*-cyclotriphosphazenes obtained from the reactions of partly substituted phosphazene (**3**) with Pyr, Pip, Morp, DASD, AEPyr, AEPip, and AEMorp.

2.3. Syntheses

2.3.1. Syntheses of the compounds (**1** and **2**)

Tyramine Schiff base {2-[(*E*)-2-(4-hydroxyphenylethyl)iminomethyl]phenol} (**1**) was prepared according to a published procedure in which salicylaldehyde was reacted with tyramine in dry MeOH [26]. The molecular structural determination of **1** has been reported [27], and a different polymorph of **1** was studied by experimental (MS, FT-IR, NMR and X-ray diffraction) and computational [density functional theory (DFT)] methods from the point of the tautomerism in solution and the solid state by our research group [28]. It was observed that the phenol-imine tautomer is predominant for tyramine Schiff base (**1**) in both DMSO solution and the solid state [28]. However, in 2-hydroxy aldimine Schiff bases, it is found as the polarity of the medium increases, the phenol-imine [(O—H. . .N), π → π* transition of the C=N group (300–340 nm)] tautomer decreases, while keto-amine [(O. . .H—N), n → π* transition of the C=O group (>400 nm)] tautomer increases [29].

Compound (**2**) was prepared from the reduction of **1** (8.80 g, 36.00 mmol) with borax (2.78 g, 7.20 mmol) and sodium borohydride (2.76 g, 73.00 mmol) in dry MeOH (300 mL). The mixture was heated at reflux for 4 h. MeOH was then evaporated and the residue was extracted with chloroform (100 mL, three times). Yield: 6.92 g (78%). mp: 99 °C. Anal. Calc. for $C_{15}H_{17}NO_2$ (%): C, 74.05; H, 7.04; N, 5.76. Found; C, 74.11; H, 7.02; N, 5.69%. IR (KBr, cm^{-1}): *ν* 2841–2800 (C—H aliph.), 1589 (C=C). ESI-MS (I_r%): *m*/*z* 244 {[*M*H]$^+$, 100}.

2.3.2. Synthesis of partly substituted spiro-cyclotriphosphazene {4′,4′,6′,6′-Tetrachloro-3-(4-hydroxyphenylethyl)-3H,4H-spiro{[1,3,2-benzoxazaphosphinine]-2,2′-[1,3,5,2,4,6]triazatriphosphinine]}} (**3**)

K_2CO_3 (7.27 g, 52.6 mmol) was added to a stirred solution of **2** (3.19 g, 13.0 mmol) in dry THF (200 mL). The mixture was heated at reflux for 4 h and then cooled to room temperature. A solution of $N_3P_3Cl_6$ (4.56 g, 13.0 mmol) in dry THF (100 mL) and triethylamine (5.30 g, 52.6 mmol) was added. The mixture was stirred for four days at ambient temperature with argon being passed over the reaction mixture. The precipitated triethylaminehydrochloride and excess of K_2CO_3 were filtered off, and the solvent was evaporated at reduced pressure. The crude product was subjected to column chromatography [silica gel 60 (230–400 mesh) (30 g) as adsorbent and toluene/THF mixture (8/1) as the eluent, *Rf* = 0.46] and crystallized from toluene/THF mixture (8/1). Yield: 4.85 g (72%). mp: 148 °C. Anal. Calc. for $C_{15}H_{15}Cl_4N_4O_2P_3$ (%): C, 34.78; H, 2.92; N, 10.82. Found; C, 34.83; H, 2.96; N, 10.73%. IR (KBr, cm^{-1}): *ν* 2958–2926 (C—H aliph.), 1589 (C=C), 1242 (asymm.), 1173 (symm.) (P=N), 593 (asymm.), 527 (symm.) (P—Cl). ESI-MS (fragments are based on ^{35}Cl, I_r%): *m*/*z* 519 {[*M*H]$^+$, 100}.

2.3.3. Syntheses of fully substituted spiro-cyclotriphosphazenes

Fully substituted *spiro*-cyclotriphosphazenes (**4a**–**g**) were prepared by similar methods; therefore, the experimental procedure of the preparation was only described in detail for the first case.

2.3.3.1. 4′,4′,6′,6′-Tetra(2-pyrrolidinyl)-3-(4-hydroxyphenylethyl)-3H,4H-spiro{[1,3,2-benzoxazaphosphinine]-2,2′-[1,3,5,2,4,6]triazatriphosphinine]} (**4a**).

A solution of Pyr (0.68 g, 9.60 mmol) in dry THF (50 mL) was added to a stirred solution of **3** (0.50 g, 0.96 mmol) in dry THF (200 mL) at room temperature. The mixture was stirred for 72 h at room temperature under argon and monitored by TLC indicating no starting material remaining. The precipitated Pyr hydrochloride was filtered off, and the solvent was evaporated. The crude product was subjected to column chromatography [silica gel 60 (230–400 mesh) (30 g) as adsorbent and toluene/THF (6/1) mixture as the eluent, R_f = 0.17] and crystallized from toluene/THF (6/1). Yield: 0.28 g (44%). mp: 78 °C. Anal. Calc. for $C_{31}H_{47}N_8O_2P_3$ (%): C, 56.70; H, 7.21; N, 17.06. Found: C, 56.64; H, 7.16; N, 17.06. IR (KBr, cm^{-1}): *ν* 2958–2848 (C—H aliph.), 1589 (C=C), 1234 (asymm.), 1190 (symm.) (P=N). ESI-MS (I_r%): *m*/*z* 657 {[*M*H]$^+$, 100}.

2.3.3.2. 4′,4′,6′,6′-Tetra(1-piperidinyl)-3-(4-hydroxyphenylethyl)-3H,4H-spiro{[1,3,2-benzoxazaphosphinine]-2,2′-[1,3,5,2,4,6]triazatriphosphinine]} (**4b**).

Compound (**4b**) was prepared from Pip (1.19 g, 14.0 mmol) and **3** (0.72 g, 1.40 mmol) (24 h), column chromatography [silica gel (30 g), toluene/THF (8/1), R_f = 0.26], crystallized from benzene/THF (2/1). Yield: 0.43 g (45%). mp: 181 °C. Anal. Calc. for $C_{35}H_{55}N_8O_2P_3$ (%): C, 58.98; H, 7.78; N, 15.72. Found: C, 59.02; H, 7.83; N, 15.68. IR (KBr, cm^{-1}): *ν* 2916–2816 (C—H aliph.), 1589 (C=C), 1261 (asymm.), 1172 (symm.) (P=N). ESI-MS (I_r%): *m*/*z* 713 {[*M*H]$^+$, 100}.

2.3.3.3. 4′,4′,6′,6′-Tetra(4-morpholinyl)-3-(4-hydroxyphenylethyl)-3H,4H-spiro{[1,3,2-benzoxazaphosphinine]-2,2′-[1,3,5,2,4,6]triazatriphosphinine]} (**4c**).

Compound (**4c**) was prepared from Morp (1.26 g, 14.5 mmol) and **3** (0.75 g, 1.45 mmol) (48 h), column chromatography [silica gel (30 g), toluene/THF (1/1), R_f = 0.35], crystallized from toluene/THF (1/1). Yield: 0.65 g (63%). mp: 170 °C. Anal. Calc. for $C_{31}H_{47}N_8O_6P_3$ (%): C, 51.66; H, 6.57; N, 15.55. Found: C, 51.64; H, 6.55; N, 15.56. IR (KBr, cm^{-1}): *ν* 2958–2846 (C—H aliph.), 1593 (C=C), 1215 (asymm.), 1170 (symm.) (P=N), 1130 (C—O). ESI-MS (I_r%): *m*/*z* 721 {[*M*H]$^+$, 100}.

2.3.3.4. 4′,4′,6′,6′-Tetra(1,4,7-dioxazonan-7-yl)-3,4-dihydro-3-(4-hydroxyphenylethyl)-3H,4H-spiro{[1,3,2-benzoxazaphosphinine]-2,2′-[1,3,5,2,4,6]triazatriphosphinine]} (**4d**).

Compound (**4d**) was prepared from DASD (2.15 g, 15.0 mmol) and **3** (0.78 g, 1.50 mmol) (48 h), column chromatography [silica gel (30 g), toluene/THF (1/1), R_f = 0.35], crystallized from toluene/THF (1/1). Yield: 0.69 g (49%). mp: 165 °C. Anal. Calc. for $C_{43}H_{63}N_8O_{10}P_3$ (%): C, 54.66; H, 6.72; N, 11.86. Found: C, 54.71; H, 6.79; N, 11.80. IR (KBr, cm^{-1}): *ν* 2949–2846 (C—H aliph.), 1591 (C=C), 1197 (P=N), 1145 (C—O). ESI-MS (I_r%): *m*/*z* 945 {[*M*H]$^+$, 100}.

2.3.3.5. 4′,4′,6′,6′-Tetra{1-[4-(2-aminoethyl)pyrrolidinyl]}-3,4-dihydro-3-(4-hydroxyphenylethyl)-3H,4H-spiro{[1,3,2-benzoxazaphosphinine]-2,2′-[1,3,5,2,4,6]triazatriphosphinine]} (**4e**).

Compound (**4e**) was prepared from AEPyr (1.61 g, 14.1 mmol) and **3** (0.73 g, 1.41 mmol) (48 h), column chromatography [silica gel (30 g), THF, R_f=0.06], obtained the oily crude product. Yield: 0.61 g (52%). Anal. Calc. for $C_{39}H_{67}N_{12}O_2P_3$ (%): C, 56.51; H, 8.15; N, 20.28. Found: C, 56.47; H, 8.12; N, 20.31. IR (KBr, cm^{-1}): *ν* 3192 (N—H), 2958–2873 (C—H aliph.), 1585 (C=C), 1230 (asymm.), 1192 (symm.) (P=N). ESI-MS (I_r%): *m*/*z* 829 {[*M*H]$^+$, 84}.

2.3.3.6. 4′,4′,6′,6′-Tetra{1-[4-(2-aminoethyl)piperidinyl]}-3,4-dihydro-3-(4-hydroxyphenylethyl)-3H,4H-spiro{[1,3,2-benzoxazaphosphinine]-2,2′-[1,3,5,2,4,6]triazatriphosphinine]} (**4f**).

Compound (**4f**) was prepared from AEPip (1.84 g, 14.3 mmol) and **3** (0.74 g, 1.43 mmol) (48 h), column chromatography [silica gel (30 g), THF, R_f = 0.08], obtained the oily crude product. Yield: 0.67 g (53%). Anal. Calc. for $C_{53}H_{75}N_{12}O_2P_3$ (%): C, 58.35; H, 8.54; N, 18.99. Found: C, 58.33; H, 8.49; N, 18.99. IR (KBr, cm^{-1}): *ν* 3207 (N—H), 2929–2800 (C—H aliph.), 1587 (C=C), 1174 (P=N). ESI-MS (I_r%): *m*/*z* 885 {[*M*H]$^+$, 40}.

2.3.3.7. 4′,4′,6′,6′-Tetra{4-[4-(2-aminoethyl)morpholinyl]}-3,4-dihydro-3-(4-hydroxyphenylethyl)-3H,4H-spiro{[1,3,2-benzoxazaphosphinine]-2,2′-[1,3,5,2,4,6]triazatriphosphinine]} (**4g**).

Compound (**4g**) was prepared from AEMorp (1.78 g, 1.37 mmol) and **3** (0.71 g, 1.37 mmol) (48 h), column chromatography [silica gel (30 g), THF, R_f = 0.10], obtained the oily crude product. Yield: 0.61 g

(48%). Anal. Calc. for $C_{39}H_{67}N_{12}O_6P_3$ (%): C, 52.46; H, 7.56; N, 18.82. Found: C, 52.38; H, 7.50; N, 18.86. IR (KBr, cm^{-1}): ν 3186 (N—H), 2953–2808 (C—H aliph.), 1587 (C=C), 1174 (P=N), 1138 (C—O). ESI-MS (I_r%): m/z 893 {[MH]$^+$, 100}.

2.4. Single crystal X-ray structure determination

The colorless crystals of compounds **3** and **4b** were crystallized from toluene/THF (8/1) and benzene/THF (2/1) at ambient temperature, respectively. Detailed crystallographic data and structure refinement parameters appear in Table 1 [30,31], while selected bond lengths and angles appear in Table S1 (S: designates supporting information). Crystallographic data were recorded on a Bruker Breeze APEXII CCD area-detector diffractometer using MoK$_\alpha$ radiation (λ = 0.71073 Å) at T = 293 K. Absorption corrections by multi-scan [32] were applied. Structures were solved by direct methods and refined by full-matrix least squares against F^2 using all data [33]. All atoms (except hydrogens) were located from a difference Fourier map and refined anisotropically. Aromatic and methylene H atoms were positioned geometrically at distances of 0.93 (CH) Å and 0.97 (CH_2) Å from the parent C atoms, and a riding model was used during the refinement process. U_{iso}(H) values were constrained to 1.2U_{eq} for methine and methylene carrier atoms. The relatively high residual in the difference Fourier map can be attributed to the disorder of C1, C8 and C28 atoms in **4b**. The C1, C8 and C28 atoms were split into C1a and C1b, C8a and C8b, C28a and C28b with site occupation factors 0.42(2) and 0.58(2), respectively.

Table 1
Crystallographic data for **3** and **4b**.

	(**3**)	(**4b**)
Chemical formula	$C_{15}H_{15}Cl_4N_4O_2P_3$	$C_{35}H_{55}N_8O_2P_3$
Colour/shape	Colorless/prism	Colorless/prism
Formula weight	518.02	712.78
F(0 0 0)	1048	764
Radiation, graphite monochr.	MoK$_\alpha$ (λ = 0.71073 Å)	MoKα (λ = 0.71073 Å)
Crystal system	Monoclinic	Triclinic
Space group	$P2_1/c$	P-1
a (Å)	16.9216(12)	10.2567(2)
b (Å)	8.9670(7)	10.3484(2)
c (Å)	16.6543(11)	18.6118(5)
α(°)	90	101.1970(10)
β(°)	119.48	103.5190(10)
γ(°)	90	93.8580(10)
Volume (Å^3)	2199.9(3)	1870.97(7)
Z	4	2
Crystal dimension (mm)	0.40 × 0.30 × 0.15	0.30 × 0.15 × 0.10
Temperature (K)	293(2)	293(2)
D_{calc} (mg m^{-3})	1.564	1.265
Abs. coefficients (mm^{-1})	0.776	0.202
T_{min}/T_{max}	0.7466/0.8925	0.9419/0.9801
Unique reflections measured	14,683	32,958
Independent reflections	6952	9005
R_{int}	0.0566	0.0310
No of reflections with I > 2 $\sigma(I)$	2778	6296
θ range (°)	2.25–28.30	2.02–28.52
Range of h, k, l	−25 < h < 19, −13 < k < 13, −24 < l < 24	−13 < h < 13, −13 < k < 13, −24 < l < 24
Refinement on	F^2	F^2
Calculated weights	$w = 1/[\sigma^2(Fo^2) + (0.0829P)^2 + 0.2178P]$ P = $(Fo^2 + 2Fc^2/3)$	$w = 1/[\sigma^2(Fo^2) + (0.0648P)^2 + 0.5434P]$ P = $(Fo^2 + 2Fc^2/3)$
Diffractometer/scan	Bruker Kappa APEX II/φ and w	Bruker Kappa APEX II/φ and w
Number of refinement parameters	253	466
S	1.046	1.026
R [$F^2 > 2\sigma(F^2)$]	0.0533	0.0478
wR (F^2)	0.1455	0.1166
$(\Delta\rho)_{max}$ (e Å^{-3})	0.781	0.445
$(\Delta\rho)_{min}$ (e Å^{-3})	−0.733	−0.282

2.5. DNA cleavage activity

The interactions of tyramine Schiff base (**1**), tyramine podand (**2**), and partly (**3**) and fully substituted (**4a**–**g**) *spiro*-cyclotriphosphazenes and starting compound ($N_3P_3Cl_6$), tyramine, Pyr, Pip, Morp, DASD, AEPyr, AEPip, and AEMorp with pBR322 plasmid DNA were studied, and the screenings of DNA–compound interactions were carried out via gel electrophoresis on a 1% agarose gel [34]. DMSO has been often used to prepare solutions of compounds with low water solubility for investigating DNA interactions [35]. In several studies, it has been shown that using minimum amounts of DMSO for the preparation of the stock solutions has no effect on nucleic acids [36]. Therefore, the compounds were dissolved in DMSO, and the resulting solutions were immediately applied to the plasmid DNA. The plasmid DNA aliquots (20 μg/mL) were incubated in the presence of increasing concentrations of the compounds by preparing [DNA] / [Compound] = R 0.3:1.0, 0.6:1.0, 1.0:1.0, 1.3:1.0 and 1.6:1.0 ratios at 37 °C for 24 h in the dark. 10 μL aliquots of compound/DNA mixtures were loaded onto 1% agarose gel with a loading buffer (0.1% bromophenol blue, 0.1% xylene cyanol), and electrophoresis was performed on Thermo Midi-cell Primo horizontal electrophoresis system in 0.05 M tris base, 0.05 M glacial acetic acid and 1 mM EDTA (TAE buffer, pH = 8.0) for 5 h at 35 V with a Thermo EC250-90 power supply. Later, the gel was stained with ethidium bromide (0.5 μg/mL) for 45 min, washed with water for 45 min, visualized under UV light using a transilluminator (DNr MiniBIS 16 mm Pro Bio-Imaging System) and photographed. The experiments were repeated three times. Untreated Supercoiled DNA was used as a control.

2.6. UV titrations

Solutions of calf thymus DNA (CT-DNA; purchased from Sigma) in 50 mM ammonium acetate (pH = 7.5) had a UV-vis absorbance ratio of 1.8–1.9:1 at 260 and 280 nm (A260 / A280 = 1.9), indicating that the DNA was sufficiently free of protein. The concentration of DNA was determined spectrophotometrically using a molar absorptivity of 6600 $M^{-1}.cm^{-1}$ (260 nm) [37]. Double-distilled water was used to prepare buffers. Stock solutions of CT-DNA were stored at 4 °C and used within 4 days. UV-vis spectra were recorded on a Carry VinUV 100 Bio, Varian spectrophotometer. The compounds were dissolved in minimum amounts of DMSO before preparing stock solutions. The absorption titrations of tyramine Schiff base (**1**), partly (**3**) and fully AEPyr (**4e**) substituted *spiro*-cyclotriphosphazenes were studied in a buffer (50 mM ammonium acetate, pH = 7.5) were performed by using a fixed compound concentration to which increments of the 3 mM DNA stock solution were added. Compound solutions employed were 200 μM in concentration and CT-DNA was added (by portions) to a ratio of 6:1 [DNA]/[Compound] and thoroughly mixed after every addition. Compound–DNA solutions were incubated for 10 min before the absorption spectra were recorded.

2.7. Molecular docking calculations

Molecular docking calculations for **3** and **4b** were performed on AutoDock Vina software [38] and AutoDockTools (ADT) was used for creating docking data entry files. The crystal data of CT-DNA were obtained from Protein Data Bank (PDB) identifiers 3V9D for

A-DNA and 1BNA for B-DNA. Both A-DNA and B-DNA are right-hand double helices, but the A-form is shorter and more compact (wider diameter, smaller rise per base pair). This is a result of a change in conformation for the deoxyribose sugar ring (C3′ in A-DNA and C2′ in B-DNA) that brings the 5′ and 3′ hydroxyls closer together, resulting in a deeper major groove and a shallower minor Groove [39]. Water molecules were removed with Discover Studio Visualizer 4.0. The molecular geometry of the compounds (**3** and **4b**) was directly taken from the X-ray diffraction experimental result of the geometry optimization. The compounds were prepared for docking by minimizing its energy at the B3LYP/6-31G level. ADT was performed to add partial charges using the Geistener method and to define torsions and rotatable bonds. The active site of the DNA was defined to include residues of active site within the grid size of 40x40x40. Receptor-ligand interactions were demonstrated with PyMol and Discover Studio Visualizer 4.0 software [40].

3. Results and discussion

3.1. Chemistry

The reaction of $N_3P_3Cl_6$ with the potassium salt of tyramine podand (**2**) led to the formation of a novel *spiro*-cyclotriphosphazene derivative (**3**). The other phenolic oxygen atom of **2** remains in a 4-hydroxyphenylethyl pendant arm without being bound to a phosphorus atom in the same or in a different cyclotriphosphazene ring. Hence, this reaction is regioselective because only the *spiro*-skeleton has been formed, instead of the other expected phosphazene architectures such as *ansa*, *bino*, *spiro*-ansa, and *spiro*-bino. Triethylamine was used to remove the liberated HCl as NEt_3.HCl in the nucleophilic substitution reaction of $N_3P_3Cl_6$ with tyramine podand (**2**). The reactions of partly substituted phosphazene (**3**) with excess heterocyclic amines (Pyr, Pip, Morp, DASD, AEPyr, AEPip, and AEMorp) in dry THF produced fully substituted *spiro*-cyclotriphosphazenes (**4a-g**), respectively (Scheme 1). An excess of the heterocyclic amine was used to scavenge the liberated HCl. Elemental analyses of the compounds are consistent with the structures, and fragments were observed under electrospray ionization mass spectrometry (ESI–MS) conditions. The mass spectrum of partly substituted phosphazene (**3**) shows a parent ion at 519 {$[MH]^+$, 100} with the expected isotope pattern. All of the fully substituted phosphazenes produced protonated molecular ions $[MH]^+$.

3.2. IR spectroscopy

The FTIR spectra of phosphazenes exhibited strong absorption frequencies in the range of 1261–1168 cm^{-1} ascribed to $\nu_{P=N}$ bands of the cyclotriphosphazene ring [41]. The most characteristic bands of the Morp, DASD and AEMorp substituted cyclotriphosphazenes were assigned to the C—O—C etheric bonds in the range of 1145–1130 cm^{-1}. Additionally, the IR spectra of AEPyr, AEPip and AEMorp substituted phosphazenes displayed N—H stretching absorptions at approximately 3200 cm^{-1}. The partly substituted *spiro*-cyclotriphosphazene (**3**) gave stretching frequencies of PCl_2 bonds [593 cm^{-1} (asymm.) and 527 cm^{-1} (symm.)]. These bands disappear in the IR spectra of fully heterocyclic amine substituted phosphazenes.

3.3. NMR spectroscopy

The signals of δOPN and δPX_2 of **4a–g** shifted upfield by 1.2–4.7 and downfield by 11.1–12.4 ppm with respect to the corresponding δOPN and δPCl_2 of **3** (Table 2). The two-bond coupling constants $^2J_{(P,P)}$ for the fully substituted phosphazenes were far smaller than those of the partly substituted one.

The ^{1}H and ^{13}C NMR resonances of *spiro*-cyclotriphosphazene derivatives **3**, and **4a–g** are assigned on the basis of chemical shifts, multiplicities and coupling constants, and summarized in Tables 3 and 4, respectively. The assignments were made unambiguously by HSQC. HSQC spectra of **4b** (Fig. S1), **4d** (Fig. S2), and **4e** (Fig. S3) are given as examples.

The ArCH_2N protons of the *spiro*-cyclotriphosphazenes were observed at ca. 4.20 ppm and give rise to doublets, and the average coupling constant, $^3J_{PH}$, was 14.7 Hz, indicating that these protons were equivalent to each other. The δ-shifts of the ArCH_2CH_2N protons of the 4-hydroxyphenylethyl pendant arm were observed at 3.27 and 3.22 ppm for **3** and **4b**, respectively, as doublets of triplet. The ^{1}H NMR spectra of the phosphazenes (**4a–g**) indicate that four substituents (Pyr, Pip, Morp, DASD, AEPyr, AEPip, and AEMorp) are bonded to phosphorus atoms. The NCH_2CH_2 and NCH_2 proton signals of the heterocyclic amines were easily distinguished from those of the *spiro* rings by the HSQC spectra of **4a–g**. In the ^{1}H NMR spectra of the heterocyclic amine-substituted compounds (**4a–g**), the substituent protons were observed as a pair of signals, indicating that the two geminal substituents are not equivalent (see a schematic representation of the phosphazenes in Table 3). This situation was observed for NCH_2CH_2 (**4a**, **4d**, **4e** and **4 g**), NCH_2CH_2 (**4a–f**), NCH_2CH_2NH (**4e** and **4 g**), NCH_2CH_2NH (**4e–g**), and OCH_2CH_2O (**4d**) protons. As expected, while the four different proton signals of the aromatic rings (H_3, H_4, H_5 and H_6) for the phosphazene derivatives were two sets of doublets and triplets, the H_8 and H_9 aromatic proton signals in the 4-hydroxyphenylethyl pendant arm were doublets of doublet (AA′BB′ spin system).

All expected carbon peaks were assigned from the ^{13}C NMR spectra of the compounds. The most reliable evidence gathered from the substitution of all Cl–atoms of partly substituted **3** was the carbon signals of the heterocyclic amine substituents. The NCH_2CH_2 and NCH_2 carbon signals of the *spiro*-rings of **4a–g** were distinguished from the corresponding carbon signals of the heterocyclic amine precursors. In the ^{13}C NMR spectra of the substituted derivatives, the geminal heterocyclic amine substituents showed two groups of $NCH_2CH_2CH_2$ (Pip, except 4**f**), NCH_2CH_2 (Pyr and Pip), NCH_2CH_2, NCH_2CH_2NH and NCH_2CH_2NH (AEPyr, AEPip and

Table 2
^{31}P NMR Data ($CDCl_3$) of **3**, and **4a–g** (δ in ppm, J in Hz).

Compound	Spin system	δ_{ClPCl}	δ_{XPX}	δ_{OPN}	$^2J_{PP}$
(**3**)	AX_2	P_X:23.71	–	P_A:0.4.80	$^2J_{AX}$:56.7
(**4a**)	AX_2	–	P_X:19.02	P_A:17.16	$^2J_{AX}$:46.6
(**4b**)	AX_2	–	P_X:22.51	P_A:16.26	$^2J_{AX}$:46.0
(**4c**)	AX_2	–	P_X:21.67	P_A:16.34	$^2J_{AX}$:47.3
(**4d**)	AX_2	–	P_X:21.45	P_A:15.94	$^2J_{AX}$:47.3
(**4e**)	AX_2	–	P_X:19.33	P_A:17.10	$^2J_{AX}$:50.7
(**4f**)	AX_2	–	P_X:19.34	P_A:16.88	$^2J_{AX}$:49.3
(**4g**)	AX_2	–	P_X:19.40	P_A:16.76	$^2J_{AX}$:49.3

Table 3
^{1}H NMR data ($CDCl_3$) of **2**, **3** and **4a–g** (δ in ppm, *J* in Hz, s: *singlet*, d: *doublet*, dd: *doublets of doublet*, t: *triplet*, b: *broad*, and m: *multiplet peak*).

H		(2)	(3)	(4a)	(4b)	(4c)	(4d)	(4e)	(4f)	(4g)
ArC***H***$_2$CH$_2$N		2.61 (m,2H)	2.86 (t,2H) $^3J_{HH}$ = 7.6	2.81 (t,2H) $^3J_{HH}$ = 8.2	2.84 (t,2H) $^3J_{HH}$ = 7.6	2.83 (t,2H) $^3J_{HH}$ = 8.2	2.79 (t,2H) $^3J_{HH}$ = 7.6	2.77 (t,2H) $^3J_{HH}$ = 6.6	2.89 (t,2H) $^3J_{HH}$ = 6.0	2.78 (t,2H) $^3J_{HH}$ = 6.0
ArCH$_2$C***H***$_2$N		2.65 (m,2H)	3.27 (m,2H)	3.22 (m,2H)	3.22 (m,2H) $^3J_{PH}$ = 15.0	3.20 (m,2H)	3.19 (m,2H)	3.15 (m,2H)	3.24 (m,2H)	3.14 (m,2H)
ArC***H***$_2$N		3.79 (s,2H)	4.18 (d,2H) $^3J_{PH}$ = 15.6	4.18 (d,2H) $^3J_{PH}$ = 14.8	4.19 (d,2H) $^3J_{PH}$ = 14.4	4.22 (d,2H) $^3J_{PH}$ = 15.2	4.14 (d,2H) $^3J_{PH}$ = 14.5	4.17 (d,2H) $^3J_{PH}$ = 14.4	4.24 (d,2H) $^3J_{PH}$ = 14.4	4.17 (d,2H) $^3J_{PH}$ = 14.4
NCH$_2$CH$_2$C***H***$_2$		–	–	–	1.51 (m,8H)	–	–	–	1.40 (m,8H)	
NCH$_2$C***H***$_2$		–	–	1.72 (m,8H) 1.78 (m,8H)	1.46 (m,16H)	3.63 (m,16H) $^3J_{PH}$ = 16.4 $^3J_{HH}$ = 4.2	1.62 (t,8H) $^3J_{HH}$ = 4.8 1.67 (t,8H) $^3J_{HH}$ = 5.0	1.65 (m,8H) 1.68 (m,8H)	1.57 (m,16H)	3.53 (t,8H) $^3J_{HH}$ = 4.4 3.61 (t,8H) $^3J_{HH}$ = 4.0
NC***H***$_2$CH$_2$		–	–	3.12 (m,8H) 3.17 (m,8H)	3.05 (m,8H) 3.10 (m,8H)	3.09 (m,8H) 3.18 (m,8H)	3.19 (m,8H) 3.26 (m,8H)	2.95 (t,8H) $^3J_{HH}$ = 5.2 2.99 (t,8H) $^3J_{HH}$ = 4.6	3.01 (t,8H) $^3J_{HH}$ = 4.8 3.05 (t,8H) $^3J_{HH}$ = 4.8	2.95 (m,16H)
NCH$_2$C***H***$_2$NH		–	–	–	–	–	–	2.45 (m,4H) 2.46 (m,4H)	2.40 (m,8H)	2.36 (m,4H) 2.40 (m,4H)
NC***H***$_2$CH$_2$NH		–	–	–	–	–	–	2.52 (m,4H) 2.54 (m,4H)	2.44 (t,4H) $^3J_{HH}$ = 5.6 2.48 (t,4H) $^3J_{HH}$ = 4.0	2.28 (m,4H) 2.37 (m,4H)
OC***H***$_2$CH$_2$O		–	–	–	–	–	3.91 (s,8H) 3.94 (s,8H)			
N***H***		–	–	–	–	–	–	4.53 (b,4H)	5.09 (b,4H)	4.44 (b,4H)
Ar$_1$O***H***		*	–	–	–	–	–	–	–	–
Ar$_7$O***H***		*	4.92 (b,1H)	*	4.69 (b,1H)	*	*	5.15 (b,1H)	*	*
Ar***H***	***H***$_3$	7.01 (d,1H)	7.01 (d,1H)	6.90 (d,1H)	6.93 (d,1H)	6.95 (d,1H)	6.93 (d,1H)	6.91 (d,1H)	7.00 (d,1H)	6.94 (d,1H)
	H$_4$	6.65 (t,1H)	7.071 (t,1H)	6.89 (t,1H)	6.91 (t,1H)	6.96 (t,1H)	6.92 (t,1H)	6.86 (t,1H)	6.94 (t,1H)	6.90 (t,1H)
	H$_5$	7.02 (t,1H)	7.25 (t,1H)	7.11 (t,1H)	7.13 (t,1H)	7.18 (t,1H)	7.15 (t,1H)	7.06 (t,1H)	7.13 (t,1H)	7.08 (t,1H)
	H$_6$	6.66 (d,1H)	7.073 (d,1H)	6.86 (d,1H)	6.88 (d,1H)	6.89 (d,1H)	6.93 (d,1H)	6.80 (d,1H)	6.87 (d,1H)	6.78 (d,1H)
	H$_8$,***H***$'_8$	6.65 (dd,2H)	6.76 (dd,2H)	6.73 (dd,2H)	6.74 (dd,2H)	6.71 (dd,2H)	6.70 (dd,2H)	6.65 (dd,2H)	6.75 (dd,2H)	6.65 (dd,2H)
	H$_9$,***H***$'_9$	6.95 (dd,2H)	7.08 (dd,2H)	6.88 (dd,2H)	6.99 (dd,2H)	6.99 (dd,2H)	6.50 (dd,2H)	6.92 (dd,2H)	7.02 (dd,2H)	6.91 (dd,2H)
	$^3J_{3-4}$	7.2	7.2	7.2	6.6	7.3	6.9	7.3	7.4	7.2
	$^3J_{4-5}$	8.4	7.6	7.6	7.2	7.2	7.6	7.6	7.5	7.7
	$^3J_{5-6}$	7.2	7.0	7.6	8.4	7.6	7.0	8.4	8.0	8.4
	$^3J_{8-9}$	8.4	8.8	8.4	8.6	8.6	8.8	8.2	8.8	8.6
	$^3J_{8-8}$	1.6	1.5	1.8	1.6	1.5	1.8	1.7	1.5	1.7
	$^3J_{9-8}$	1.5	1.7	1.6	1.7	1.5	1.6	1.8	1.6	1.7

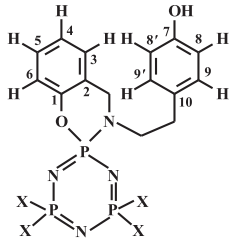

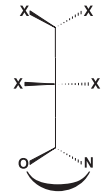

Schemetic representative structure of the phosphazenes

* Not observed.

Table 4
^{13}C NMR data ($CDCl_3$) of **2**, **3** and **4a–g** (δ in ppm, J in Hz).

C		(2)	(3)	(4a)	(4b)	(4c)	(4d)	(4e)	(4f)	(4g)
Ar***C***H_2CH_2N		35.2	34.1 $^3J_{PC}$ = 2.3	34.4 $^3J_{PC}$ = 3.9	34.4 $^3J_{PC}$ = 4.5	34.4 $^3J_{PC}$ = 4.5	34.5	40.2	37.7	37.5
$ArCH_2$***C***H_2N		50.9	50.4 $^2J_{PC}$ = 3.8	50.4 $^2J_{PC}$ = 2.5	50.2 $^2J_{PC}$ = 2.1	50.1 $^2J_{PC}$ = 3.2	50.2	49.9	49.9	50.0
Ar***C***H_2N		51.3	49.1 $^2J_{PC}$ = 3.8	49.2	49.2	49.0	49.1	48.7	48.8	48.9
NCH_2CH_2***C***H_2		–	–	–	25.0 25.1	–	–	–	24.2	–
NCH_2***C***H_2		–	–	26.4 $^3J_{PC}$ = 11.0	26.3 $^3J_{PC}$ = 7.5	67.2 $^3J_{PC}$ = 7.0	35.5	23.3 23.4	25.6 25.7	66.7 66.8
N***C***H_2CH_2		–	–	46.1 46.2	45.2 45.3	44.6	42.6	39.4	37.5	37.2
NCH_2***C***H_2NH		–	–	–	–	–	–	53.8 53.9 54.0	54.2 54.3 54.5	53.3 53.4 53.5
N***C***H_2CH_2NH		–	–	–	–	–	–	57.1 $^3J_{PC}$ = 7.8 57.2 $^3J_{PC}$ = 7.8 58.2	59.1 59.69 $^3J_{PC}$ = 7.0 59.72 $^3J_{PC}$ = 7.0	59.25 $^3J_{PC}$ = 7.8 59.34 $^3J_{PC}$ = 7.8
O***C***H_2CH_2O		–	–	–	–	–	64.2	–	–	–
O***C***O		–	–	–	–	–	107.5 107.8	–	–	–
Ar***C***	C_1	156.2	149.9 $^2J_{PC}$ = 8.4	151.7 $^2J_{PC}$ = 7.8	151.7 $^2J_{PC}$ = 8.5	151.3 $^2J_{PC}$ = 8.4	151.6 $^2J_{PC}$ = 8.4	151.6 $^2J_{PC}$ = 7.8	151.6 $^2J_{PC}$ = 7.7	151.3 $^2J_{PC}$ = 7.8
	C_2	124.8	124.1 $^3J_{PC}$ = 6.9	124.9 $^3J_{PC}$ = 7.8	124.9 $^3J_{PC}$ = 7.7	124.7 $^3J_{PC}$ = 7.8	124.7 $^3J_{PC}$ = 7.7	124.1 $^3J_{PC}$ = 7.8	124.2 $^3J_{PC}$ = 7.7	124.1 $^3J_{PC}$ = 7.7
	C_3	128.5	126.5	126.5	126.5	126.7	126.5	126.6	126.6	126.7
	C_4	116.0	124.3	122.2	122.2	122.8	122.4	122.3	122.3	122.6
	C_5	129.2	129.0	127.8	127.8	128.2	128.0	127.9	128.1	128.2
	C_6	119.1	118.7 $^3J_{PC}$ = 8.6	118.4 $^3J_{PC}$ = 7.8	118.3 $^3J_{PC}$ = 7.7	118.3 $^3J_{PC}$ = 7.8	118.5 $^3J_{PC}$ = 7.0	118.3 $^3J_{PC}$ = 7.1	118.3 $^3J_{PC}$ = 6.9	118.2 $^3J_{PC}$ = 7.8
	C_7	158.1	154.3	155.2	154.6	154.7	154.7	155.9	155.8	155.7
	C_8,C_8	115.8	115.5	115.7	115.5	115.6	115.5	115.7	115.8	115.6
	C_9,C_9	130.1	130.0	129.3	129.6	129.7	129.8	129.6	129.6	129.5
	C_{10}	130.6	130.6	130.6	130.6	130.8	130.8	130.1	130.1	130.1

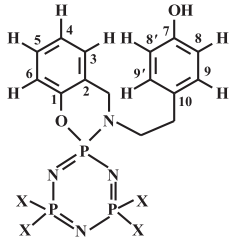

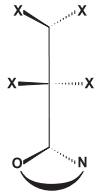

Schemetic representative structure of the phosphazenes

AEMorp), and OCO (DASD) (Table 4). The results also indicate that the two geminal heterocyclic amine groups were not equivalent to each other.

3.4. X-ray crystallography

The crystallographic data and selected bond lengths and angles of **3** and **4b** are listed in Table 1 and Table S1, respectively. Figs. 1 and 2, respectively, illustrate the molecular structures of **3** and **4b** along with the atom-numbering schemes. The intermolecular O—H…N^{i} hydrogen bond [O2—H20 (0.820(3) Å); H20…N1^{i} (2.210(3) Å); O2…N1^{i} (2.901(4) Å); O2–H20…N1^{i} (142.04 (0.22)°); symmetry code: (i) x, −y + 1/2, +z + 1/2 for **3**, and O2—H2 (0.835(3) Å); H2…N3^{i} (2.056(4) Å); O2…N3^{i} (2.876(2) Å); O2—H2…N3^{i} (167.38(3.29)°); symmetry code: (i) x, y − 1, +z] for **4b** linked cyclotriphosphazene molecules, and dipole-dipole and van der Waals interactions were important in molecular packing (Figs. S4 and S5, respectively).

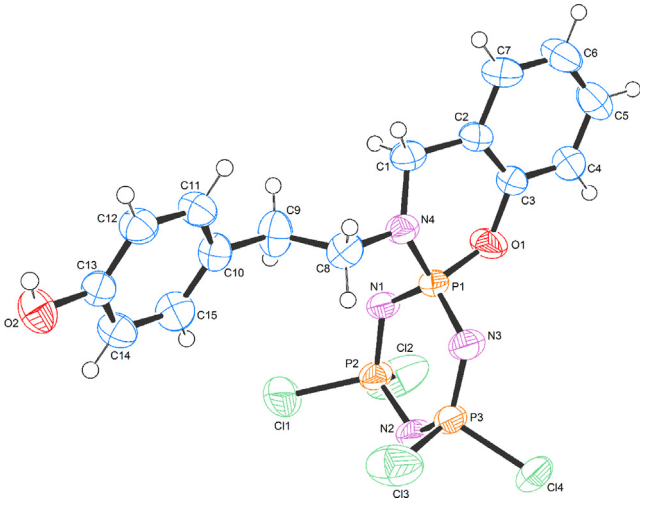

Fig. 1. ORTEP-3 drawing of **3** with the atom-numbering scheme. Displacement ellipsoids are drawn at the 30% probability level.

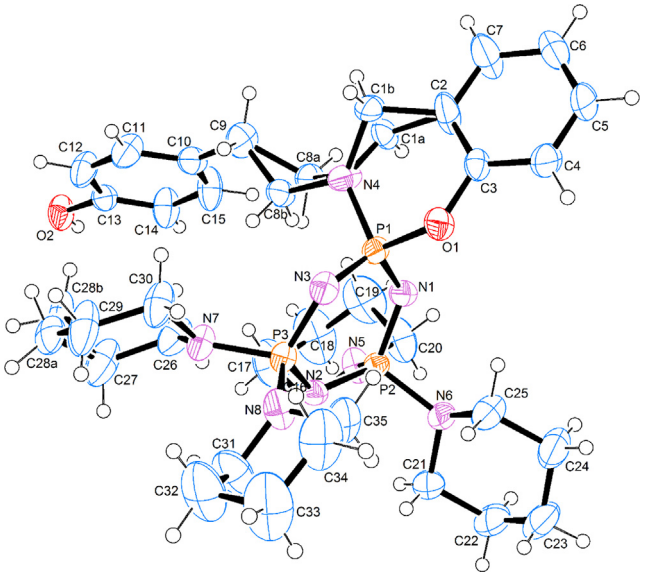

Fig. 2. ORTEP-3 drawing of **4b** with the atom-numbering scheme. Displacement ellipsoids are drawn at the 30% probability level.

The phosphazene ring of **3** and **4b** adopts a flattened-boat conformation [Fig. S6-A(a), φ_2 = 36.4(1)°, θ_2 = 102.5(1)° for **3** and Fig. S6-B(a), φ_2 = 46.4(4)°, θ_2 = 75.9(4)° for **4b** (*P*1/N1/*P*2/N2/*P*3/N3)] with total puckering amplitude [42] Q_T of 0.200(2) Å (for **3**) and Q_T of 0.205(1) Å (for **4b**). In **3**, the six-membered *spiro* ring (*P*1/N4/C1/*C*2/C3/O1) adopts a twisted conformation [Fig. S6-A (b), Q_T = 0.355(4) Å, φ_2 = 160.6(1)°, θ_2 = 109.7(1)°]. The relatively high residual in the difference Fourier map can be attributed to the disorder of C1 in the six-membered *spiro* ring (*P*1/N4/C1/*C*2/C3/O1) of **4b**. The C1 atom is split into C1a and C1b with site occupation factors of 0.58(2) and 0.42(2), respectively. In **4b**, the six-membered *spiro* ring (*P*1/N4/C1a/*C*2/C3/O1 and *P*1/N4/C1b/*C*2/C3/O) adopts a twisted conformation [Fig. S6-B(b), Q_T = 0.354(4) Å, φ_2 = 152.3(4)°, θ_2 = 123.2(3)° (for *P*1/N4/C1a/C2/C3/O1) and Q_T = 0.523(3) Å, φ_2 = 13.1(2)°, θ_2 = 81.8.(3)° (for *P*1/N4/C1b/*C*2/C3/O)].

In the literature, the PN single and double bonds are generally in the ranges of 1.628–1.691 Å and 1.571–1.604 Å, respectively [43]. The endocyclic PN bond lengths of **3** (1.561(3)–1.604(3) Å) and **4b** (1.5742(16)–1.6166(17) Å) (see Table S1) are in agreement with these findings. The average endocyclic PN bond lengths of **3** and **4b** are 1.579(3) and 1.5924(16) Å, respectively, which are considerably shorter than the exocyclic PN bond of **3** [1.614(3) Å] and the average exocyclic PN bonds of **4b** [1.6546(17) Å]. Variations in the endocyclic NPN bond angles are very large, ranging from 112.83(14)° to 124.61(16)° (for **3**) and 116.41(8)° to 123.80(10)° (for **4b**) with an average value of 119.44(16)° and 119.43(9)°, respectively. The endocyclic NPN bond angle for the P–atom containing *spiro* substituent is much affected by the tyramine podand (**2**) bonded to the P-atom, while the exocyclic NPN bond angles are less affected compared to the corresponding angle [118.3(2)°] [44] in the "standard" compound $N_3P_3Cl_6$. On the other hand, the values of endocyclic N1–P1–N3 and exocyclic N4–P1–O1 angles of tetra Pip substituted **4b** are bigger and smaller than those of the starting tetrachloro *spiro*-cyclotriphosphazene **3**, respectively. Based on the electron releasing capacities of the substituents for **3** and **4b**, electrons are transferred from Pip groups to the cyclotriphosphazene ring in **4b**. Moreover, the endocyclic P1–N1–P2 angle of **3** is noticeably narrow, but, the other endocyclic PNP angles of **3** and all the endocyclic PNP angles of **4b** are slightly large with respect to the corresponding value of $N_3P_3Cl_6$ [121.4(3)°] [44].

3.5. The relationship between ^{31}P NMR and X-ray crystallography

Shaw first noted relationships between the angles around the P-atoms and ^{31}P NMR spectral data in phosphazenes [45]. The variations of δP-shifts depend on the variety of the angles around the P-atoms, and on steric and electronic factors (for example the conformation and electron-releasing and the -withdrawing capacities of small or bulky substituents and the steric hindrance of exocyclic groups) of the phosphazene derivatives. A systematic study using ^{31}P NMR spectral and X-ray crystallographic data of **3** and **4b** and cyclotriphosphazenes possessing six-membered *spiro* ring/rings (P/N/$C_{Aliph.}$/$C_{Arom.}$/$C_{Arom.}$/O) (**I**–**V**) in the literature [46–61] (Table 5) has revealed correlations between structural parameters. These correlations include the relationships δP_{OPN} shifts with exocyclic OPN bond angles (α′) [Fig. 3)], electron density transfer parameters Δ(P-N) [Fig. 4 (X)], and endocyclic NPN bond angles (α) [Fig. 4 (Y)]. The OPN (α′) and NPN (α) bond angles, and the bond lengths (a, a′, b and b′) on the general formulae of the *spiro*-cyclotriphosphazenes are marked in Table 5 and δP_{OPN} shifts, α and α′ bond angles, and Δ(P-N) values are listed in Table 6. Approximate linearity between δP_{OPN} shifts and α′ bond angles is observed for four groups of cyclotriphosphazenes [(a)–(d)] given in Fig. 3. When comparing partly [(a) and (b)] substituted phosphazenes with the fully heterocyclic amine-substituted ones [(c) and (d)], changes in α′ bond angles are more sensitive to changes in δP_{OPN} shifts

Table 5
The exocyclic OPN bond angles (α′) and bond lengths (a, a′, b and b′) on the formulae of cyclotriphosphazenes possessing six-membered *spiro* ring/rings (P/N/$C_{Aliph.}$/$C_{Arom.}$/$C_{Arom.}$/O) in the literature.

spiro-Phosphazene	−Ar−	X	R	No[Ref]	*spiro*-Phosphazene	−Ar−	X	R	No[Ref]
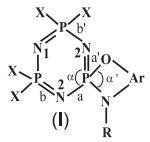 (I)		Cl	CH_3	**Ia**[46]	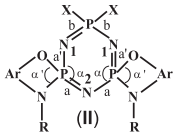 (II)		Cl	$CH_3CH_2CH_2$	**IIa**[47]
		Cl	CH_3CH_2	**Ib**[47]			N	$CH(CH_3)_2$	**IIb**[46]
		Cl	$CH_3CH_2CH_2$	**Ic**[47]			N		**IIc**[46]
		Cl		**Id**[48]	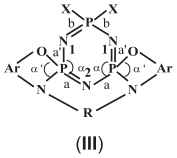 (III)		Cl	CH_2CH_2	**IIIa**[54,55]
		Cl		**Ie**[46]			Cl	$CH_2CH_2CH_2CH_2$	**IIIb**[55,56]
		Cl		**If**[49]			N	CH_2CH_2	**IIIc**[57,58]
		Cl		**1g**[49,50]			N O	CH_2CH_2	**IIId**[57]
		Cl		**Ih**[51,52]				CH_2CH_2	**IIIe**[57,59]
		N		**Ii**[53]	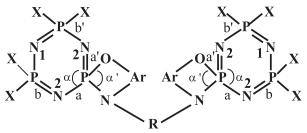 (IV)		Cl	$CH_2CH_2CH_2$	**IVa**[55]
		Cl		**Ij**[53]			N O	CH_2CH_2	**IVb**[57]
		N		**Ik**[53]	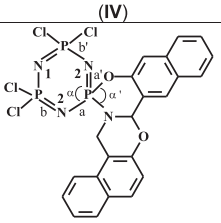 (V)[60,61]				
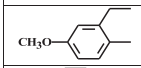		Cl		**Il**[53]					
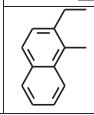		Cl	H	**Im**[47]					

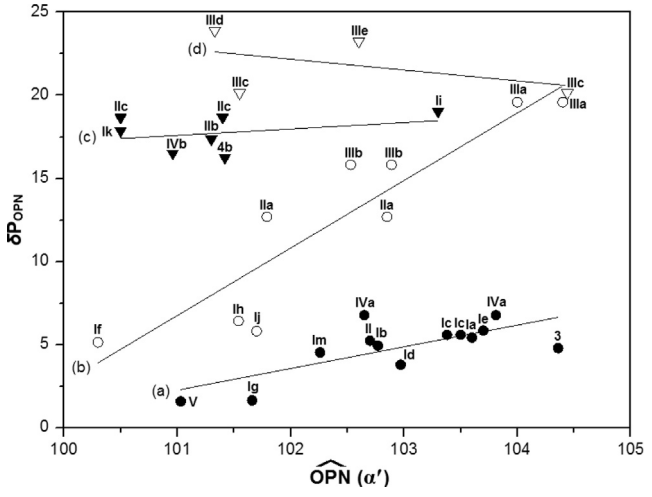

Fig. 3. The relationship between exocyclic OPN bond angles (α′) and δP_{OPN} shifts for (a) and (b) the partly substituted, and (c) and (d) the fully heterocyclic amine-substituted six-membered *spiro*-cyclotriphosphazenes.

for partly substituted phosphazenes, due to the weaker steric interaction between Cl-atoms than that between bulky heterocyclic amine groups. Especially for group (b) phosphazenes, relatively small changes in α′ bond angles cause significant changes in δP_{OPN} shifts.

The electron density transfer parameters Δ(P-N), which are the difference between the bond lengths of two adjacent endocyclic PN bonds [Δ(a–b)], and are calculated from the equations given in Table 6 for the *spiro*-cyclotriphosphazenes, provides a measure of the electron-releasing and -withdrawing capacities of the substituents bonded to the P-atoms of cyclotriphosphazene rings [62]. A "cluster" of points rather than linear trend has been observed between Δ(P-N) and δP_{OPN} shifts. In Fig. 4 (X), one can easily observe for all of the structural types are accumulated in regions A, B and C, respectively. As expected, when Δ(P-N) value is increasing, the substituents bonded to the P–atoms withdraw electrons from the cyclotriphosphazene ring. Shortening of the exocyclic P-O and P-N bonds is likely to be a measure of the electron-withdrawing capacities of the substituents. When this value is decreasing, substituents bonded to the P-atoms release electrons to the cyclotriphosphazene ring and, hence, the electron density around the P—N bonds in cyclotriphosphazene ring increases, which is likely to be a measure of the increase in negative hyperconjugation [63,64]. In order to make sense of this relationship, the basicity of the phosphazene ring nitrogen atoms (N1 and N2 marked in Table 5) in partly substituted cyclotriphosphazenes [(**3**), (**Ia-h**, **Ij**, **Il**, **Im**), (**IIa**, **IIIa**) and (**IVa**)] with those in fully substituted ones [(**4a**), (**Ii**, **Ik**), (**IIb**, **IIc**), (**IIIb-d**) and (**IVb**)] can be compared. The basicity of the ring nitrogens depends on electron-donating and electron-withdrawing groups. Thus, the basicity of N2 atom/atoms in partly substituted phosphazenes seems to have increased due to electron-withdrawing capacity of the chloro groups, while N1 atom/atoms in fully substituted derivatives, indicating that the electron densities of the P_{OPN} atoms of partly substituted derivatives increase which can be attributed to the presence of the negative hyperconjugation. The same trend in the opposite direction is interestingly observed between α bond angles and δP_{OPN} shifts [Fig. 4(Y)].

Consequently, while the electron-releasing groups bonded to the P–atoms decrease the negative hyperconjugation of the PN bonds, the electron-withdrawing groups increase the multiple-bond character of the PN bonds. Therefore, the narrowing and broadening of the exocyclic OPN (α′) and endocyclic NPN (α) bond

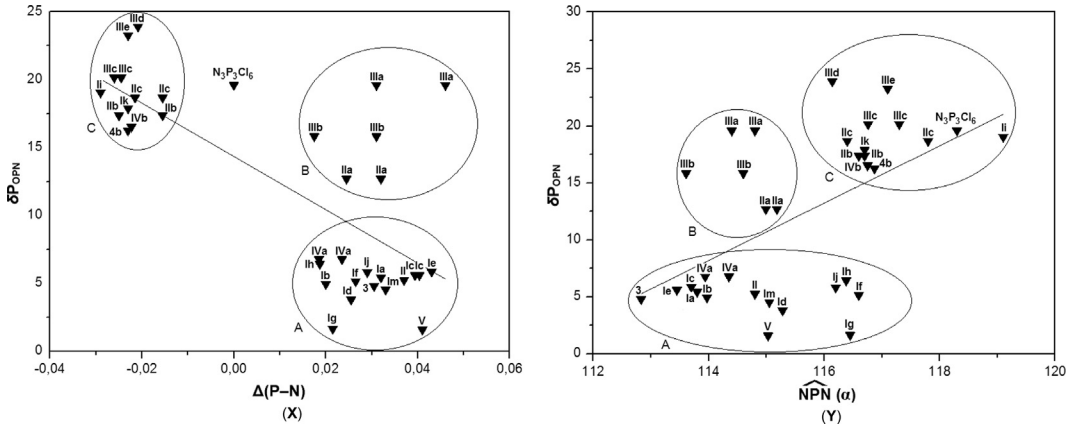

Fig. 4. The relationship between (**X**) Δ(P-N) values and δP_{OPN} shifts, and (**Y**) endocyclic NPN bond angles (α) and δP_{OPN} shifts for the partly and fully heterocyclic amine substituted *spiro*-cyclotriphosphazenes. δP_{ClPCl} shift and the α value of $N_3P_3Cl_6$ is 19.60 ppm and 118.3(2)°, respectively [44].

Table 6
Exoxcyclic OPN bond angles (α′), bond lengths (a, a′, b and b′), δP_{OPN} shifts and Δ(P-N) values for the compounds [δP_{OPN}(*spiro*) shifts in ppm, α and α′ angles in °, a, a′, b and b′ lengths in Å].

Compound	a	a′	b	b′	Δ(P-N)	α′	α	δP_{OPN}	
3	1.604(3)	1.589(3)	1.566(3)	1.566(3)	0.0305	104.36(13)	112.83(14)	4.80	for (**3**), (**4b**), (**I**), (**IV**) and (**V**)
4b	1.5916(18)	1.5742(16)	1.6166(17)	1.5953(15)	−0.02305	101.42(8)	116.82(8)	16.26	$\Delta(P-N)=\frac{a+a'}{2}-\frac{b+b'}{2}$
Ia	1.588(4)	1.587(3)	1.555(4)	1.556(3)	0.032	103.6(2)	113.8(2)	5.44	for (**II**) and (**III**)
Ib	1.589(3)	1.603(3)	1.603(3)	1.549(3)	0.020	102.77(15)	113.97(14)	4.95	$\Delta(P-N)=\frac{a+a'}{2}-b$
Ic	1.598(7)	1.589(7)	1.5513(94)	1.555(7)	0.04035	103.50(4)	113.45(0.35)	5.60	
	1.596(7)	1.596(7)	1.5566(76)	1.556(7)	0.0394	103.38(0.36)			
Id	1.583(3)	1.600(3)	1.569(3)	1.563(3)	0.0255	102.97(13)	115.28(15)	3.80	
Ie	1.591(3)	1.596(3)	1.548(3)	1.553(3)	0.043	103.7(2)	113.7(2)	5.86	
If	1.589(4)	1.597(4)	1.564(3)	1.569(3)	0.0265	100.3(2)	116.6(2)	5.15	
Ig	1.584(3)	1.582(3)	1.558(3)	1.565(3)	0.0215	101.66(13)	116.45(14)	1.66	
Ih	1.584(2)	1.592(2)	1.5743(12)	1.5643(19)	0.0187	101.54(9)	116.38(11)	6.43	
Ii	1.583(2)	1.575(2)	1.606(2)	1.610(4)	−0.029	103.3(1)	119.1(1)	19.04	
Ij	1.605(1)	1.592(1)	1.565(1)	1.574(1)	0.029	101.7(1)	116.2(1)	5.82	
Ik	1.577(2)	1.583(2)	1.606(2)	1.600(2)	−0.023	100.5(1)	116.7(1)	17.88	
Il	1.604(2)	1.594(2)	1.557(2)	1.567(2)	0.037	102.7(1)	114.8(1)	5.25	
Im	1.599(4)	1.584(4)	1.559(4)	1.558(4)	0.033	102.26(19)	115.05(2)	4.54	
IIa	1.566(3)	1.5981(3)	1.550(3)	–	0.032	101.79(15)	115.18(15)	12.70	
	1.582(3)	1.583(3)	1.558(3)	–	0.0245	102.85(15)	114.99(15)		
IIb	1.593(2)	1.571(2)	1.607(1)	–	−0.025	101.3(1)	116.7(1)	17.37	
	1.588(1)	1.591(1)	1.605(1)	–	−0.0155	101.3(1)	116.6(1)		
IIc	1.579(2)	1.580(2)	1.601(2)	–	−0.0215	100.5(1)	117.8(1)	18.67	
	1.596(2)	1.577(2)	1.602(2)	–	−0.0155	101.4(1)	116.4(1)		
IIIa	1.588(5)	1.602(5)	1.564(5)	–	0.031	104.0(3)	114.8(3)	19.59	
	1.579(5)	1.621(6)	1.554(5)	–	0.046	104.4(2)	114.4(3)		
IIIb	1.570(3)	1.605(3)	1.570(3)	–	0.0175	102.53(16)	113.61(15)	15.83	
	1.579(3)	1.603(3)	1.560(3)	–	0.0310	102.89(14)	114.60(15)		
IIIc	1.585(3)	1.577(3)	1.607(3)	–	−0.0260	101.55(16)	117.30(16)	20.15	
	1.584(3)	1.567(3)	1.600(3)	–	−0.0245	104.44(15)	116.76(16)		
IIId	1.5811(18)	1.5890(19)	1.6059(18)	–	−0.02085	101.33(10)	116.14(10)	23.90	
IIIe	1.577(5)	1.585(4)	1.604(4)	–	−0.0230	102.6(2)	117.1(2)	23.25	
IVa	1.589(5)	1.594(5)	1.573(6)	1.563(5)	0.0235	103.81(17)	114.35(19)	6.78	
	1.582(6)	1.575(5)	1.554(6)	1.566(5)	0.0185	102.65(15)	113.94(18)		
IVb	1.5715(39)	1.5843(30)	1.6008(34)	1.5996(30)	−0.0223	100.96(17)	116.75(18)	16.53	
V	1.607(3)	1.592(3)	1.554(3)	1.563(3)	0.041	101.03(14)	115.03(17)	1.60	
$N_3P_3Cl_6$[58]						101.2(1)	118.3(2)	19.60	

angles, and the shortening of the PN and PO bonds of **3** and **4b** may reflect the steric hindrances of the side groups and may be referred to the substituent-depended charges at the P-centers indicating the electronic and steric properties of the substituents and negative hyperconjugation.

3.6. Interactions of DNA with the compounds

When circular plasmid DNA is subjected to electrophoresis, relatively fast migration is observed in the intact supercoiled form (Form I). If a scission occurs on one strand (nicked circular), then the supercoil form relaxes to generate a slower-moving open circu-

Fig. 5. Electrophoretograms of the interaction of pBR322 plasmid DNA with 500 μM concentration of tyramine (line 2), salicylaldehyde (line 3), tyramine Schiff base (**1**) (line 4), tyramimine podand (**2**) (line 5), Pyr (line 6), Pip (line 7), Morp (line 8), DASD (line 9), AEPyr (line 10), AEPip (line 11), and AEMorp (line 12). Line 1 is the control line: only pBR322 plasmid DNA, no compounds were added. Three bands from top to bottom correspond to form II (single nicked open circular), form III (linear) and form I (covalently closed circular or supercoiled) plasmids, respectively.

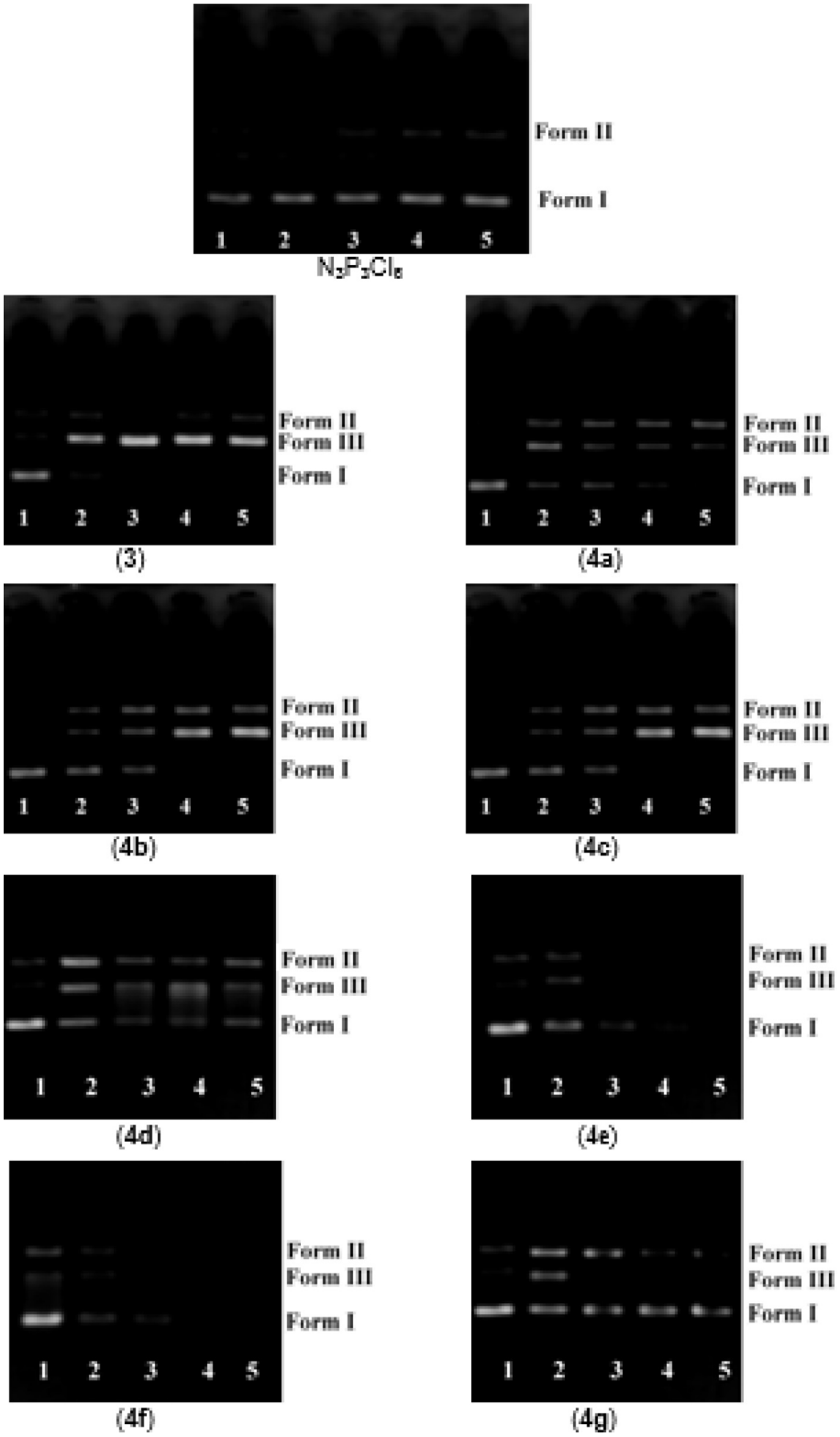

Fig. 6. Electrophoretograms of the interaction of pBR322 plasmid DNA with increasing concentrations of $N_3P_3Cl_6$, **3**, and **4a**–**g**. Untreated pBR322 plasmid DNA was applied to lane 1. Concentrations (in μM) are as follows: lanes 2–5 apply to plasmid DNA interacting with increasing concentrations of the compounds (lane 2: 100; lane 3: 200; lane 4: 300; lane 5: 400). Three bands from top to bottom correspond to form II (single nicked open circular), form III (linear) and form I (covalently closed circular or supercoiled) plasmids, respectively.

lar form (Form II). If both strands are cleaved, a linear form (Form III) that migrates between forms I and II is generated [65]. In Figs. 5 and 6, line 1 is the control line where no compounds have been added to the pBR322 plasmid DNA. There is mainly one band at the lowest level, which is supercoiled DNA (Form I) and a very low amount of the nicked DNA (Form II) just above it. When multiple scissions occur in both strands, then fast-moving small DNA pieces are formed.

pBR322 was exposed to the starting compounds tyramine, salicylaldehyde, tyramine Schiff base (**1**), tyramimine podand (**2**), heterocyclic amines (Pyr, Pip, Morp, DASD, AEPyr, AEPip, and AEMorp) at the highest concentration (500 μM), and Fig. 5 shows the separation of pBR322 DNA by gel electrophoresis after incubation with these starting compounds. Salicylaldehyde shows some degree of DNAse activity, but tyramine schiff base (**1**) completely changes pBR322′s supercoiled conformation into Form II and mostly Form III. Tyramine podand (**2**) has very little effect, turning a small portion of DNA into Form II. All of the other heterocyclic amines had no effect on DNA. Fig. 6 gives the electrophoretograms generated from incubated mixtures of pBR322 DNA at varying concentrations (400 to 100 μM) of the phosphazenes [starting compound $N_3P_3Cl_6$, and synthesized compounds (**3**, and **4a**–**g**)]. $N_3P_3Cl_6$ has a very slightly effect on pBR322, producing increasing amounts of Form II as the concentration of the compound increases. Partly substituted cyclotriphosphazene **3** completely changed the conformation of pBR322 to Form III indicating substantial scission effect. Heterocyclic amine-substituted cyclotriphosphazene derivatives (**4a**–**g**) also have a substantial effect on pBR322 conformation. Fully Pyr substituted phosphazene (**4a**) gradually consumed the Form I as the concentration increases producing equal amounts of Form II and Form III. However, fully Pip (**4b**) and Morp (**4c**) substituted phosphazenes produced mainly form III. Fully DASD (**4d**) and AEMorp (**4g**) substituted derivatives produced a very little of form II and Form III and a high proportion of Form I still remains even at the highest concentration indicating their low scission power. In the case of fully AEPyr (**4e**) and AEPip (**4f**) substituted phosphazenes, compounds created multiple scissions on the pBR322 and all forms of DNA disappeared from the gel indicating the highest power. If the compounds were put in the order of the scission power:

4e = **4f** > **3** > **4b** = **4c** > **4a** > **4g** > **4d**

Partly substituted phosphazene (**3**) induced significantly increased damage to plasmid DNA, changing its conformation totally in its linear form. When a variety of different amines were added to **3**, only **4e** and **4f** carrying flexible aminoethylpyrrolidine and aminoethylpiperidine moieties, respectively, have improved DNAse activity, likely because of the amine functional group (—NH—CH_2—CH_2—) interacting with the negatively charged phosphate backbone of DNA. The other more rigid amine moieties had a milder effect. UV-vis titration studies revealed that the binding strength was improved by 7 times when the amine functional groups (Pyr, Pip, Morp, DASD, AEPyr, AEPip, and AEMorp) were introduced into the partly substituted phosphazene structure (**3**). By gel electrophoresis, **4e** and **4f** caused the highest level of damage with total disappearance of plasmid DNA from the gel being observed at high concentrations of the compounds.

3.7. UV titrations

Because of solubility problems, only tyramine Schiff base (**1**), and partly (**3**) and fully AEPyr (**4e**) substituted cyclotriphosphazenes were investigated by UV titration method. A 73% hypochromicity on the absorbance at 393 nm and a 20% hypochromicity at 275 nm were observed in the UV spectrum of the tyramine Schiff base (**1**) upon titration with CT-DNA (Fig. 7).

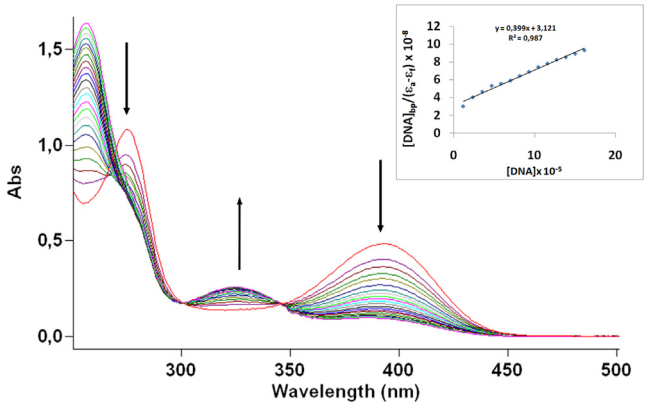

Fig. 7. Absorption spectra of tyramine Schiff base (**1**) in 50 mM ammonium acetate buffer on the addition of CT-DNA: 20 μM (**1**), 0–32 μM DNA. Arrows show the absorbance changing with increase of DNA concentration. The insets show plots of DNA concentration divided by the difference between the apparent absorption coefficient (ε_A) and the absorption coefficient of the free Schiff base (**1**), (ε_f) versus DNA concentration for the titration of DNA to Schiff base (**1**).

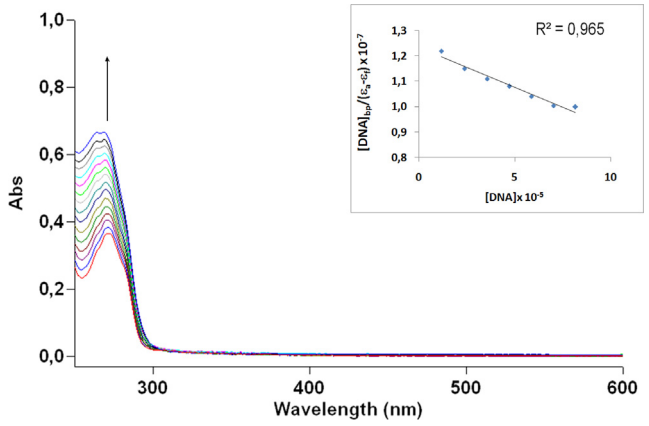

Fig. 8. Absorption spectra of compound (**3**) in 50 mM ammonium acetate buffer on the addition of CT-DNA: 20 μM (**3**), 0–32 μM DNA. Arrows show the absorbance changing with increase of DNA concentration. The insets show plots of DNA concentration divided by the difference between the apparent absorption coefficient (ε_A) and the absorption coefficient of the free compound (**3**), (ε_f) versus DNA concentration for the titration of DNA to compound (**3**).

Occurrence of the new peak at 324 nm indicates that there is a new interaction between DNA and **1**. The calculated K_b value of $1.31 \times 10^4\ M^{-1}$ indicates a moderate strength of binding. The UV spectrum of partly substituted *spiro*-cyclotriphosphazene (**3**) exhibited a 78.5% hyperchromicity at 271 nm upon addition of CT-DNA (Fig. 8). The binding constant K_b was calculated as $2.58 \times 10^3\ M^{-1}$. Hyperchromicity in the UV spectrum indicates that **3** binds to DNA as a groove binder and/or a partial intercalation with a low binding [66,67]. Fully AEPyr substituted phosphazene derivative (**4e**) also binds as a groove binder which was revealed by the 3% hyperchromicity at 273 nm in its UV spectrum upon addition of CT-DNA (Fig. 9). The binding constant value of $1.67 \times 10^4\ M^{-1}$ indicates a moderate binding strength of the compound. The addition of the 2-aminoethyl moiety onto the cyclotriphosphazene backbone, as expected, increased the binding ability of the compound presumably because the introduction of amine groups allow interactions with the negatively charged phosphate backbone of DNA.

3.8. Molecular docking study

Molecular docking can be used to model the interactions between a molecule and a DNA at the atomic level. The molecular docking study was performed to understand the interaction of compounds **3** and **4b** with and A-DNA and B-DNA. To evaluate the quality of docking results, it is common to calculate the Root Mean Square Deviation (RMSD) between the docked pose and the known crystal structure confirmation. Docking results are acceptable when the RMSD value is lower than 2 Å [68]. The predicted bonding energy as a result of molecular docking and RMSD values are given in Table S2. According to the calculated bonding affinities, these results show that the phosphazenes (**3** and **4b**) inhibit the DNA. The energetically most favorable docked structures obtained from the rigid molecular docking of **3** and **4b** with A-DNA (PDB ID: 3V9D) and B-DNA (PDB ID: 1BNA) are shown in Fig. 10. The relative binding energy of docked **3**-A-DNA, ligand **3**-B-DNA, **4b**-A-DNA, and **4b**-B-DNA were found to be −7.2, −7.9, −7,7 and −7.4 kcal/mol, respectively. Phosphazenes **3** and **4b** bind at the active site of the 3V9D for A-DNA and 1BNA for B-DNA by weak non-covalent interactions most prominent of which are H-bonding, π-σ, π-anion, CH…O for **3**-A-DNA, H-bonding, π-donor, CH…O, CH…N, negative-negative (N…O) interactions for **3**-B-DNA, π-σ, π-π, π-alkyl, CH…O, CH…N, negative-negative (N…O) for **4b**-A-DNA, and π-π, π-alkyl, CH…N for **4b**-A-DNA (Table S3). The binding interactions are illustrated in Fig. 11. Resulting docked pose of **3**-A-DNA and **3**-B-DNA, OP2 of DC4 gives H-bond with O2 atom of the hydroxyl group (2.57 Å for A-DNA, 2.96 Å for B-DNA), and OP1 of DA8 gives also H-bond N2 atom of the phosphazene ring (3.32 Å for A-DNA).

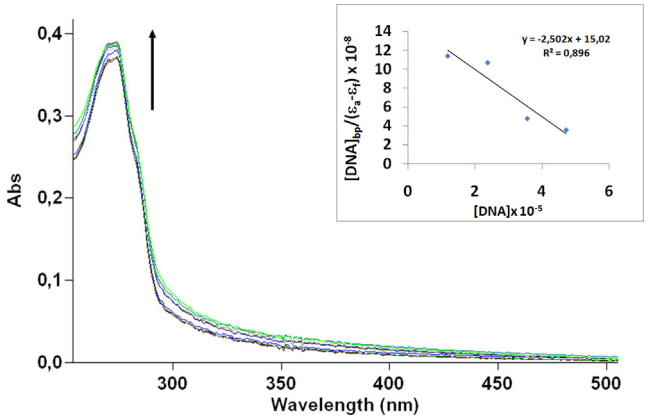

Fig. 9. Absorption spectra of compound (**4e**) in 50 mM ammonium acetate buffer on the addition of CT-DNA: 20 μM (**4e**), 0–32 μM DNA. Arrows show the absorbance changing with increase of DNA concentration. The insets show plots of DNA concentration divided by the difference between the apparent absorption coefficient (ε_A) and the absorption coefficient of the free compound (**4e**), (ε_f) versus DNA concentration for the titration of DNA to compound (**4e**).

4. Conclusions

In this paper, the partly substituted phosphazene **3** was obtained from the reaction of $N_3P_3Cl_6$ with the tyramine podand (**2**). All of the Cl atoms of **3** were then substituted with Pyr, Pip, Morp, DASD, AEPyr, AEPip, and AEMorp groups to give fully heterocyclic amine-substituted cyclotriphosphazenes **4a–g**. The relationships between δP_{OPN} shifts, α and α′ bond angles, and Δ(P-N) values were presented. Phosphazene derivatives (**3** and **4a–g**) have a substantial effect on the pBR322 conformation, and especially fully AEPyr (**4e**) and AEPip (**4f**) substituted derivatives which

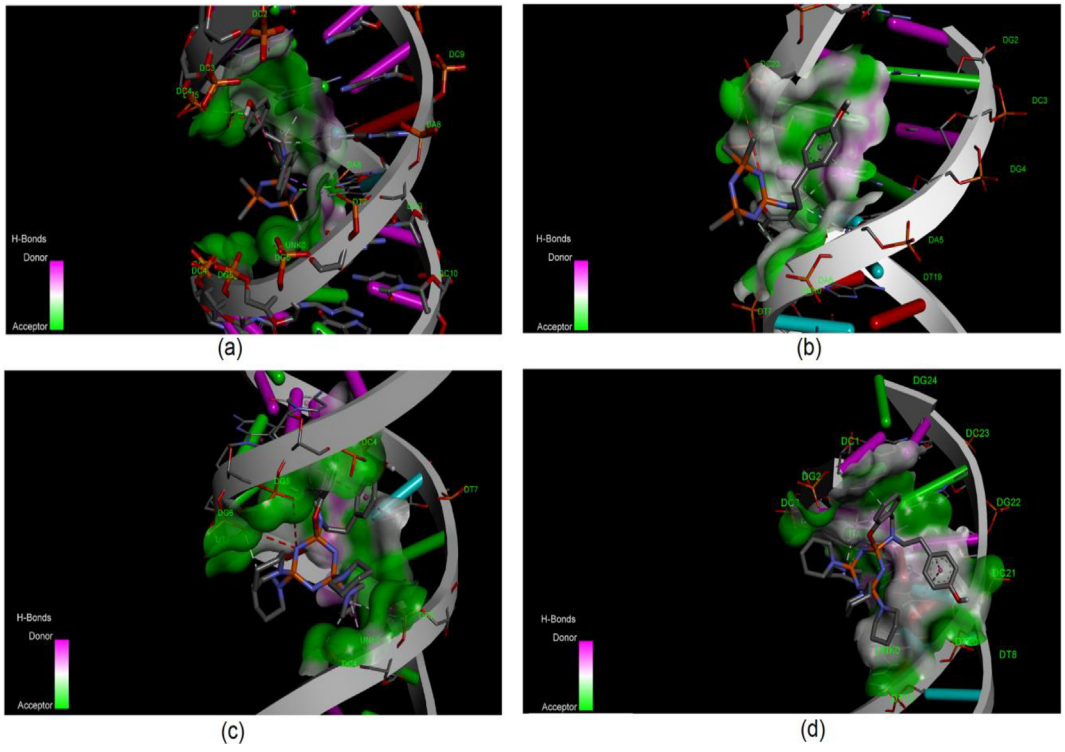

Fig. 10. Docked conformations of compounds (a) **3** with A-DNA, (b) **3** with B-DNA, (c) **4b** with A-DNA and (d) **4b** with B-DNA.

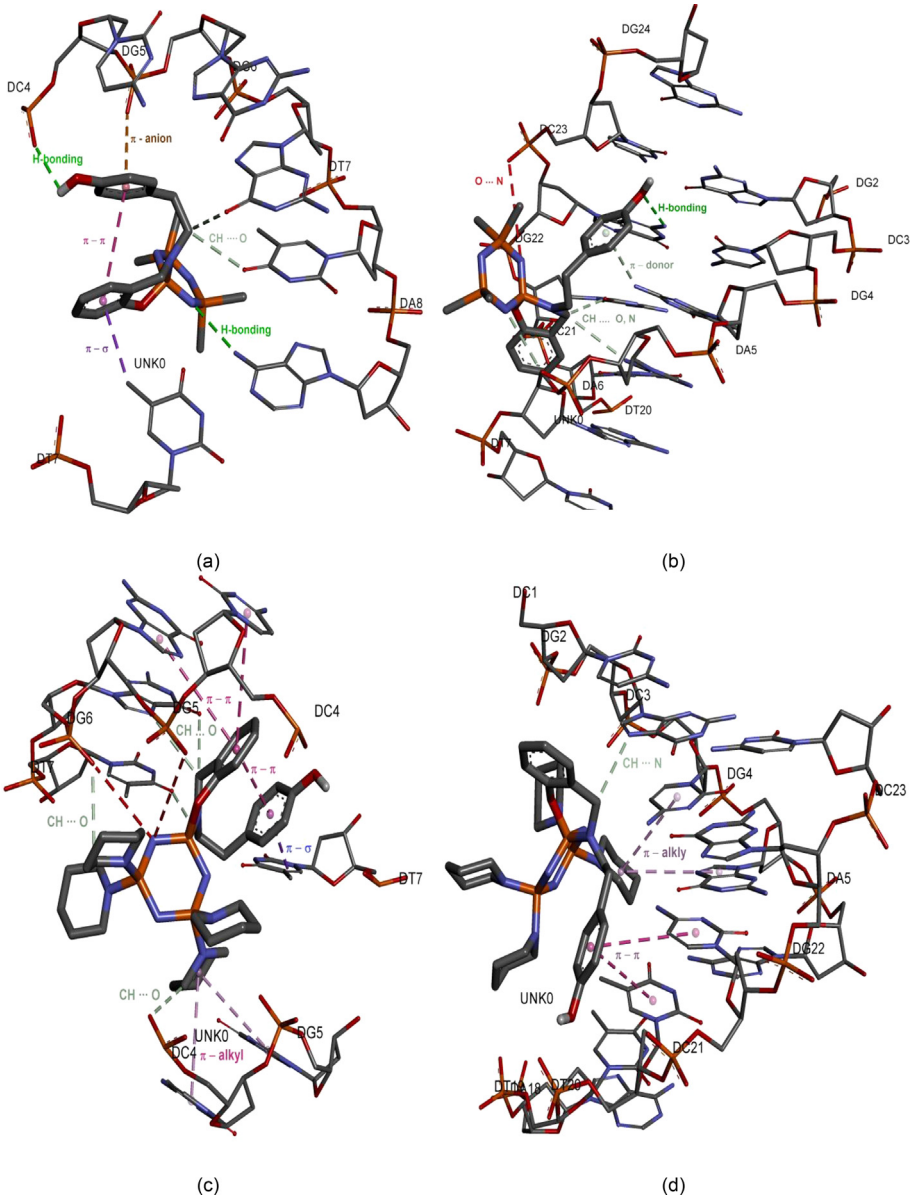

Fig. 11. Binding interactions of the compounds (a) **3** with A-DNA, (b) **3** with B-DNA, (c) **4b** with A-DNA and (d) **4b** with B-DNA.

caused the highest level of DNA damage. The DNA binding of **3** and **4e** to CT-DNA was studied by UV-vis absorption titration and the calculated binding constant values suggest moderate intercalative binding modes between the compounds and DNA. The energetically most favorable docked structures have been obtained from the rigid molecular docking of **3** and **4b** with 3V9D (A-DNA) and 1BNA (B-DNA). The compounds, **3** and **4b**, bind at the active site of the A-DNA and B-DNA by weak non-covalent interactions. The molecular docking results also suggest that **3** and **4b** exhibit binding effect against DNA; however further tests should be done to validate the computational predictions. The findings of this study may thus benefit the development of effective applications in medicine and biochemistry.

Acknowledgment

The authors would like to express their deep sense of gratitude and heartiest thanks to The Scientific and Technological Research Council of Turkey (TÜBİTAK) – Turkey (Project No. 113Z861).

Appendix A. Supplementary data

Supplementary data associated with this article can be found, in the online version, at https://doi.org/10.1016/j.ica.2018.01.016. These data include MOL files and InChiKeys of the most important compounds described in this article.

References

[1] C.W. Allen, in: R. Steudel (Ed.), Studies in Inorganic Chemistry, Elsevier, The Netherlands, Amsterdam, 1992, pp. 171–191.
[2] M. Gleria, R. De Jaeger, Phosphazenes: A Worldwide Insight, Nova Science Publishers Inc, Hauppauge, New York, USA, 2004.
[3] V.L. Furer, A.E. Vandyukov, S. Fuchs, J.P. Majoral, A.M. Caminade, V.I. Kovalenko, J. Mol. Struct. 1051 (2013) 197–204.
[4] S. Bilge, Turk. J. Chem. 35 (2011) 745–756.
[5] H. İbişoğlu, S. Beşli, F. Yüksel, İ. Ün, A. Kılıç, Inorg. Chim. Acta 409 (2014) 216–226.
[6] A. Uslu, E. Özcan, S. Dural, S. Yüksel, Polyhedron 117 (2016) 394–403.
[7] G. Egemen, M. Hayvalı, Z. Kılıç, A.O. Solak, Z. Üstündağ, J. Porphyr. Phthalocya. 14 (2010) 1–8.
[8] N. Asmafiliz, Z. Kılıç, M. Civan, O. Avcı, L.Y. Gönder, L. Açık, B. Aydın, M. Türk, T. Hökelek, New J. Chem. 40 (2016) 9609–9626.

[9] K. Kajiyama, M. Suziki, M. Kojima, Y. Setone, Inorg. Chem. Commun. 35 (2013) 330–332.
[10] G. Elmas, A. Okumuş, Z. Kılıç, L.Y. Gönder, L. Açık, T. Hökelek, J. Turk. Chem. Soc. A. 3 (2016) 26–45.
[11] Z. Song, Y. Liang, M. Fan, F. Zhou, W. Liu, Tribol. Int. 70 (2014) 136–141.
[12] J. Jiménez, I. Pintre, E. Gascón, C. Sánchez-Somolinos, R. Alcalá, E. Cavero, J.L. Serrano, L. Oriol, Macromol. Chem. Physic. 215 (2014) 1551–1562.
[13] M.-J. Xu, G.-R. Xu, Y. Leng, B. Li, Polym. Degrad. Stabil. 123 (2016) 105–114.
[14] T. Nishimoto, T. Yasuda, S.Y. Lee, R. Kondo, C. Adachi, Mater. Horiz. 1 (2014) 264–269.
[15] T. Dagger, C. Luerenbaum, F.M. Schappacher, M. WinteR, J. Power Sources 342 (2017) 266–272.
[16] G. Jacob, A. Gamboa, A. Diedrich, C. Shibao, D. Robertson, I. Biaggioni, Hypertension 46 (2005) 355–359.
[17] B.J. McCabe-Sellers, C.G. Staggs, M.L. Bogle, J. Food Compos. Anal. 19 (2006) S58–S65.
[18] M. Angela, B. De Las Rivas, J.M. Landete, L. Tabera, R. Muñoz, Crit. Rev. Food Sci. 52 (2012) 448–467.
[19] A.R. Shalaby, Food Res. Int. 29 (1996) 675–690.
[20] T. Roeder, Annu. Rev. Entomol. 50 (2005) 447–477.
[21] N. Raman, S. Sobha, L. Mitu, Monatsh. Chem. 143 (2012) 1019–1030.
[22] O. Rolland, C.-O. Turrin, G. Bacquet, R. Poupot, M. Poupot, A.-M. Caminade, J.-P. Majoral, Tetrahedron Lett. 50 (2009) 2078–2082.
[23] H. Akbaş, A. Okumuş, Z. Kılıç, T. Hökelek, Y. Süzen, L.Y. Koç, L. Açık, Z.B. Çelik, Eur. J. Med. Chem. 70 (2013) 294–307.
[24] Y. Tümer, N. Asmafiliz, Z. Kılıç, T. Hökelek, L.Y. Koç, L. Açık, M.L. Yola, A.O. Solak, Y. Öner, D. Dündar, M. Yavuz, J. Mol. Struct. 1049 (2013) 112–124.
[25] A. Okumuş, H. Akbaş, Z. Kılıç, L.Y. Koç, L. Açık, B. Aydın, M. Türk, T. Hökelek, H. Dal, Res. Chem. Intermed. 42 (2016) 4221–4251.
[26] K.S. Rajan, M.S. Rajan, S. Mainer, F.H. Jarke, J.M. DavieS, J. Inorg. Nucl. Chem. 41 (1979) 1513–1519.
[27] Y.-G. Li, H.-L. Zhu, W.-Q. Huang, L. Ai, Acta Crystallogr. E 62 (2006) o689–o690.
[28] C.T. Zeyrek, S. Bilge Koçak, H. Ünver, S. Pektaş, N.S. Başterzi, Ö. Çelik, J. Mol. Struct. 1100 (2015) 570–581.
[29] S. Bilge, Z. Kılıç, Z. Hayvalı, T. Hökelek, S. Safran, J. Chem. Sci. 121 (2009) 989–1001.
[30] L.J. Farrugia, J. Appl. Crystallogr. 30 (1997) 565–566.
[31] J.A. Ibers, W.C. Hamilton (Eds.), International Tables for X-Ray Crystallography, Birmingham: Kynoch Press (Present Distributor: Kluwer Academic Publisher, Dordrecht, The Netherlands), 1974; Vol. IV.
[32] Bruker. SADABS. Bruker AXS Inc, Madison, Wisconsin, USA, 2005.
[33] G.M. Sheldrick, SHELXS-97 and SHELXL-97, University of Göttingen, Germany, 1997.
[34] A. Okumuş, Z. Kılıç, T. Hökelek, H. Dal, L. Açık, Y. Öner, L.Y. Koç, Polyhedron 30 (2011) 2896–2907.
[35] A.N. Wein, A.T. Stockhausen, K.I. Hardcastle, M.R. Saadein, S. Peng, D. Wang, D. M. Shin, Z. Chen, J.F. Eichler, J. Inorg. Biochem. 105 (2011) 663–668.
[36] Q.İ. Zhou, P. Yang, Inorg. Chim. Acta 359 (2006) 1200–1206.
[37] B. Coban, U. Yildiz, A. Sengul, J. Biol. Inorg. Chem. 18 (2013) 461–471.
[38] A.D. Becke, J. Chem. Phys. 104 (1996) 1040–1046.
[39] O. Trott, A.J. Olson, J. Comput. Chem. 31 (2010) 455–461.
[40] S.C. Harvey, J. Struct. Biol. 189 (2015) 1–8.
[41] B. Özgüç, S. Bilge, N. Çaylak, Ş. Demiriz, H. İşler, M. Hayvalı, Z. Kılıç, T. Hökelek, J. Mol. Struct. 748 (2005) 39–47.
[42] D. Cremer, J.A. Pople, J. Am. Chem. Soc. 97 (1975) 1354–1358.
[43] F.H. Allen, O. Kennard, D.G. Watson, L. Brammer, G. Orpen, R.J. Taylor, J. Chem. Soc. Perkin Trans. 2 (12) (1987) S1–S19.
[44] G.J. Bullen, J. Chem, Soc. A (1971) 1450–1453.
[45] R.A. Shaw, Phosphorus, Sulfur Silicon Relat. Elem. 28 (1986) 99–128.
[46] M. Işıklan, N. Asmafiliz, E.E. Özalp, E.E. İlter, Z. Kılıç, B. Coşut, S. Yeşilot, A. Kılıç, A. Öztürk, T. Hökelek, L.Y. Koç Bilir, L. Açık, E. Akyüz, Inorg. Chem. 49 (2010) 7057–7071.
[47] E.E. İlter, N. Asmafiliz, M. Işıklan, Z. Kılıç, T. Hökelek, N. Çaylak, E. Şahin, Inorg. Chem. 46 (2007) 9931–9944.
[48] M. Işıklan, O. Sonkaya, B. Coşut, S. Yeşilot, T. Hökelek, Polyhedron 29 (2010) 1612–1618.
[49] H. Dal, S. Safran, Y. Süzen, T. Hökelek, Z. Kılıç, J. Mol. Struct. 753 (2005) 84–91.
[50] B. Tercan, T. Hökelek, H. Dal, Y. Süzen, Z. Kılıç, Acta Crystallogr. C 60 (2004) o639–o641.
[51] N. Çaylak, T. Hökelek, O. Büyükgüngör, H. Dal, Y. Süzen, Z. Kılıç, Acta Crystalogr. E 61 (2005) o1557–o1560.
[52] H. Dal, Y. Süzen, Spectrochim. Acta A 67 (2007) 1392–1397.
[53] N. Asmafiliz, Z. Kılıç, Z. Hayvalı, L. Açık, T. Hökelek, H. Dal, Spectrochim. Acta A 86 (2012) 214–223.
[54] B. Tercan, T. Hökelek, S. Bilge, A. Natsagdorj, Ş. Demiriz, Z. Kılıç, Acta Crystallogr. E 60 (2004) o795–o797.
[55] S. Bilge, A. Natsagdorj, Ş. Demiriz, N. Çaylak, Z. Kılıç, T. Hökelek, Helv. Chim. Acta 87 (2004) 2088–2099.
[56] N.S. Başterzi, S. Bilge Koçak, A. Okumuş, Z. Kılıç, T. Hökelek, Ö. Çelik, M. Türk, L. Y. Koç, L. Açık, B. Aydın, New J. Chem. 39 (2015) 8825–8839.
[57] S. Bilge Koçak, S. Koçoğlu, A. Okumuş, Z. Kılıç, A. Öztürk, T. Hökelek, Y. Öner, L. Açık, Inorg. Chim Acta 406 (2013) 160–170.
[58] B. Tercan, T. Hökelek, O. Büyükgüngör, S. Bilge, A. Okumuş, Z. Kılıç, Anal. Sci. 23 (2007) x121–x122.
[59] S. Bilge, Ş. Demiriz, A. Okumuş, Z. Kılıç, B. Tercan, T. Hökelek, O. Büyükgüngör, Inorg. Chem. 45 (2006) 8755–8767.
[60] B. Tercan, T. Hökelek, M. Işıklan, E.E. İlter, Z. Kılıç, Acta Crystallogr. E 60 (2004) o971–o973.
[61] E.E. İlter, N. Çaylak, M. Işıklan, N. Asmafiliz, Z. Kılıç, T. Hökelek, J. Mol. Struct. 697 (2004) 119–129.
[62] Z. Kılıç, A. Okumuş, Ş. Demiriz, S. Bilge, A. Öztürk, N. Çaylak, T. Hökelek, J. Incl. Phenom. Macrocycl. Chem. 65 (2009) 269–286.
[63] S.S. Krishnamurthy, Phosphorus, Sulfur Silicon Relat. Elem. 87 (1994) 101–111.
[64] R.J. Davidson, E.W. Ainscough, A.M. Brodie, J.A. Harrison, M.R. Waterland, Eur. J. Inorg. Chem. (2010) 1619–1625.
[65] E.E. İlter, N. Asmafiliz, Z. Kılıç, L. Açık, M. Yavuz, E.B. Bali, A.O. Solak, F. Büyükkaya, H. Dal, T. Hökelek, Polyhedron 29 (2010) 2933–2944.
[66] N. Shahabadi, L. Heidari, Spectrochim. Acta A 97 (2012) 406–410.
[67] R. Vijayalakshmi, M. Kanthimathi, V. Subramanian, B.U. Nair, Biochim. Biophys. Acta 1475 (2000) 157–162.
[68] B. Kramer, M. Rarey, T. Lengauer, Proteins Struct. Funct. Genet. 37 (1999) 228–241.